Gravitational atoms in the braneworld scenario

Sunil Singh Bohra,[1,†] Subhodeep Sarkar,[1,2,*] and Anjan Ananda Sen[1,‡]
[1]Center For Theoretical Physics, Jamia Millia Islamia, New Delhi—10025, India
[2]Indian Institute of Information Technology, Allahabad, Prayagraj, Uttar Pradesh—211015, India

(Received 18 December 2023; accepted 28 March 2024; published 7 May 2024)

In the Randall-Sundrum (RS) II braneworld scenario, general relativity (GR) is modified by adding an extra dimension such that it is indistinguishable from GR in the weak gravity limit. However, such modifications may leave a mark in the strong field regime. We therefore analyze massive scalar perturbations around rotating black holes in the RS II model. Unlike black holes in GR, these braneworld black holes carry a tidal charge that contains information about the extra spatial dimension, and the rotation parameter for such black holes can exceed unity. Through the method of continued fractions, we investigate the quasinormal mode spectra, and the superradiant instabilities associated with the existence of quasibound states, that is, gravitational atoms. In comparison to the four-dimensional Kerr black hole, we report distinctive signatures of the tidal charge and the rotation parameter, which manifest as signals of the extra dimension, on both the fundamental quasinormal mode and the formation of gravitational atoms. These findings offer insights into testing modifications to GR and detecting ultralight bosonic particles around black holes.

DOI: 10.1103/PhysRevD.109.104021

I. INTRODUCTION

The first direct detection of gravitational waves emitted during the merger of binary black holes and neutron stars [1–3], along with the recent measurements related to the shadows of supermassive black hole candidates likes M87* and Sgr A* located at the center of the Messier 87 and the Milky Way galaxies respectively [4–10] as well as the observation of relativistic effects in the orbits of stars around Sgr A* [11–13], has led to a renaissance in testing gravity in the strong field regime [14–26]. To understand classical gravitational interactions, one usually turns to Einstein's general theory of relativity (GR) which is extremely successful as far as solar system experiments, or weak gravitational fields, are concerned [27–30]. These recent breakthroughs have now confirmed that the predictions of GR agree with observations to an unprecedented degree even in the strong field regime [11–13,31–40], adding enormous heft to decades of progress made in this direction [41–44]. In the near future, pulsar timing arrays and space-borne gravitational wave detectors are expected to put GR to even more stringent tests [41,45–51]. But of course, this whole enterprise is not without its caveats and one must exercise due caution while interpreting the results [43,52–56].

Moreover, in spite of its tremendous success across various orders of the length scale, there are both theoretical and observational aspects of general relativity and black holes (BHs) that motivate us to consider alternatives to Einstein's theory. Such modified theories of gravity are usually invoked to address issues like the existence of spacetime singularities [57–59], the existence of Cauchy horizons and the breakdown of determinism in GR [60–69], the information loss paradox [70–72], explain the accelerated expansion of the universe [73–77], or the behavior of galactic rotation curves [78,79]. But when it comes to modifying gravity, we seem to be limited only by our imagination [43,80–84]. However, such alternative theories must be at par with GR when it comes to satisfying tests of gravity, both in the local and strong field regime, which is a tall order. We now know that it is indeed possible to consistently modify the Einstein-Hilbert action such that we end up with theories which can address one or more of these issues while keeping the local physics unchanged. Some popular alternatives to GR include $f(R)$ theories [85,86], Lanczos-Lovelock models [87], bimetric gravity [88–90], Horndeski [91–93] and generalized Proca theories [94–96].

In the present work, we focus on one such modification to Einstein's theory which incorporates the presence of a warped extra spatial dimension,[1] the so-called braneworld scenario [98–123], and try to infer its imprints in the strong

*Corresponding author: subhodeep.sarkar1@gmail.com
†sunilsinghbohra87@gmail.com
‡aasen@jmi.ac.in

[1]The existence of different kinds of extra spatial dimensions have been invoked by physicists in variety of contexts over the years, starting from the works of Kaluza and Klein [97] in their attempt to unify classical electromagnetism and general relativity. We refer the reader to [98] for a complete account.

field regime by studying the behavior of massive scalar field perturbations around a rotating black hole solution of the said modified theory.

Here we specifically consider the Randall Sundrum braneworld scenario, where we model the universe as a four dimensional ($4D$) spacetime (or a 3-brane) embedded in a five dimensional ($5D$) anti–de Sitter spacetime called the bulk, the extra dimension being spacelike and warped [99,100]. In such models, the matter fields are confined to the brane and only gravitational interactions can probe the bulk. The braneworld paradigm was initially proposed as a solution to the hierarchy problem in particle physics [99]. However, Randall and Sundrum proposed a second model, colloquially known as the RS-II model [100], where the observable universe is a 3-brane with a positive tension embedded in the $5D$ bulk spacetime with a warped noncompact extra dimension and a negative cosmological constant. It is particularly interesting to note that such a model can give rise to the familiar Newtonian gravitational potential on the 3-brane [100]. It was also demonstrated that the such a theory is able to reproduce the features of $4D$ Einstein gravity in the low energy limit [103–108] and numerical black hole solutions in the bulk were explored in [102] (also see Refs. [124–126]). Interestingly enough, the RS-II model can also give rise to analytical black hole solutions on the brane [111,112] that at first sight look superficially familiar to the well known black hole solutions in general relativity.

In fact, the rotating braneworld BH metric resembles that of the Kerr-Newman (KN) black hole [112]. But the solution is far from trivial since, unlike the KN solution, the braneworld solution corresponds to a vacuum solution. Moreover, the tidal charge, bearing the signature of the extra dimension, can take on both positive and negative values (unlike the electric charge). It is also important to stress that unlike KN BHs of general relativity, the braneworld BH can be *superspinning*, that is, they can possess angular momentum greater than the BH mass. Note that the black holes in our universe are supposed to be electrically neutral. But even then electrically charged black holes are routinely studied because they serve as theoretical laboratories to probe various classical and quantum aspects of gravity [127]. Therefore, by using the braneworld BH solution, one can often directly leverage existing techniques to investigate the consequences of the braneworld scenario in the context of gravitational interactions. Such an endeavor is important because it will complement the popular program to search for extra dimensions through particle physics experiments which may be inadequate to probe the presence of the noncompact extra dimension built into the RS-II model [128]. Against this backdrop, workers have studied the imprint of the tidal charge on lensing and BH shadows [129–136], BH perturbations and gravitational waves [137–154], and have explored various other aspects [155–164] as well.

In this work, we choose to explore two hitherto unexplored avenues: (i) the quasinormal mode spectra of massive scalar perturbations, and (ii) the existence of quasibound states and the associated superradiant instability, or the gravitational atom, in the braneworld scenario. We focus on the regime $\mu M < 1$ such that one obtains boson condensates around the black hole, forming a scalar gravitational atom, μ being the mass of the scalar field and M being the BH mass that sets a characteristic length scale of the problem.

To the best of our knowledge, the existence of gravitational atoms in the context of braneworld black holes has not been examined before, and this work represents the first step in a program to study the implications of the presence of a noncompact extra dimension on the behavior of boson clouds in binary black hole systems.

The paper is organized as follows. In Sec. II we introduce the rotating braneworld BH metric and discuss the region of the parameter space under exploration. In Sec. III, we discuss the wave equation governing massive scalar perturbation and elucidate the boundary conditions required for studying quasinormal modes (QNMs) and quasibound states (QBSs). We then discuss the numerical method in Sec. IV and delineate a strategy to solve the continued fraction using a simple root finding algorithm that guarantees results up to the desired degree of accuracy. We present our results in Sec. V where we first analyze the stability of the braneworld BH under massive scalar perturbations, highlighting interesting aspects of the QNM spectrum, followed by a thorough analysis of the quasibound states and the associated superradiant instability. Finally, we conclude with a few remarks in VI.

Notations and conventions: We set the fundamental constants G and c to unity. Throughout this paper, we will use the mostly positive signature convention, such that the Minkowski spacetime will have the metric $\eta_{\mu\nu} = \mathrm{diag}(-1, 1, 1, 1)$. In our numerical computations, we set the characteristic length scale given by the BH mass M to unity.

II. ROTATING BLACK HOLE IN THE BRANEWORLD SCENARIO

We had remarked that the rotating braneworld BH resembles the Kerr-Newman BH, and to understand this aspect we must look at how one arrives at the braneworld black hole metric which is a solution to the (effective) Einstein field equations on the brane [103–106]. So, in order to construct black hole solutions localized on the brane, one starts with the assumption that the $5D$ Einstein field equations are satisfied by the bulk spacetime. Then, by using an appropriate projector to the brane, and the Gauss-Codazzi relations, one can figure out the $4D$ Einstein field equations on the brane. In fact, if the bulk spacetime is empty and there are no matter fields present on the brane,

then the effective gravitational field equations on the brane are given by [103–106]

$$^{(4)}R_{\mu\nu} = -E_{\mu\nu}, \qquad ^{(4)}L^{\mu}_{\mu} = E^{\mu}_{\mu} = 0, \tag{2.1}$$

where $^{(4)}R_{\mu\nu}$ is the $4D$ Ricci tensor and $E_{\mu\nu}$ is traceless electric part of the $5D$ Weyl tensor. Therefore, from (2.1) it is clear that it is the bulk Weyl tensor that ushers in the modifications to the vacuum Einstein field equations due to the presence of the extra spatial dimension [103,106,110]. Now, one can show that $E_{\mu\nu}$ is divergenceless as well if one considers a vacuum brane [106]. Therefore, the effective vacuum braneworld field equations closely resemble those of the Einstein-Maxwell system. Dadhich *et al.* [111] used this observation to consistently map the Reissner-Nordström solution in GR to an exact static spherically symmetric black hole solution localized on a brane, and soon afterward the technique was generalized to construct a stationary and axisymmetric solution of the vacuum braneworld field equations describing a charged rotating black hole localized on a 3-brane [112], the charge being an induced *tidal charge*, inherited from the $5D$ Weyl tensor, encoding nonlocal gravitational effects from the higher dimensional bulk spacetime.

Formally, the line element for a rotating black hole in the second Randall-Sundrum (RS-II) braneworld scenario [112–114], with mass M and angular momentum $J \equiv aM$ in the usual Boyer- Lindquist coordinates, is given by,

$$ds^2 = -\frac{\Delta}{\Sigma}(dt - a\sin^2\theta d\phi)^2 + \Sigma\left(\frac{dr^2}{\Delta} + d\theta^2\right) + \frac{\sin^2\theta}{\Sigma}(adt - (r^2 + a^2)d\phi)^2, \tag{2.2}$$

where the metric functions Δ and Σ have the form,

$$\Delta = r^2 + a^2 - 2Mr - \beta, \quad \text{and} \quad \Sigma = r^2 + a^2\cos^2\theta, \tag{2.3}$$

and β is the tidal charge inherited from the bulk Weyl tensor. The tidal charge β appears in the metric even though there is no electric charge on the brane and its origin lies in nonlocal Coulomb-type effects present in the bulk space [111,112]. It is important to note that β can take on both positive and negative values, and it is evident that for negative values of β, the line element (2.2) resembles the standard Kerr-Newman solution of the Einstein-Maxwell system in GR,[2] and for $\beta = 0$ we simply recover the celebrated Kerr solution. Therefore, positive values of β differentiates this black hole solution from the standard solutions in general relativity and carries the imprint of the extra dimension. In fact, in the context of braneworld models, a positive value of β is physically more favorable [102,103,109]. We should also stress that the tidal charge is a property of the spacetime geometry itself and is different from a black hole hair, which is to say that it is similar to how the cosmological constant is a property of an asymptotically de Sitter black hole spacetime and has the same value for all such black holes, whereas a black hole hair like the mass M, or electric charge Q can be different for different black holes in the universe. The rotating braneworld black hole is therefore clearly quite distinct from its GR counterpart despite the superficial similarity. Moreover, the presence of the tidal charge β permits us to explore those values of the black hole rotation parameter a that are not allowed in GR. This fact is evident from examining the roots of $\Delta(r) = (r - r_+)(r - r_-) = 0$, viz.,

$$r_\pm = M \pm k, \tag{2.4}$$

where $k \equiv \sqrt{M^2 - a^2 + \beta}$.

The black hole will have an outer event horizon described by the largest root r_+ provided,

$$(a/M)^2 \leq 1 + \beta/M^2, \tag{2.5}$$

where the equality in the above relation corresponds to the case where $r_+ = r_- = M$, that is, in the extremal limit when the two horizons will coincide. The violation of (2.5) results in a spacetime harboring a naked singularity. Now, for the BH to achieve extremality, it is evident that for positive values of β, we must allow for the possibility $a/M \geq 1$, a situation that is forbidden for black holes in Einstein's general theory of relativity and hence one that is not discussed while studying rotating black holes in GR. Therefore, to explore effects arising out of modifications to general relativity, one has to explore the regime where the rotation parameter a is greater than the mass M of the black hole in presence of a tidal charge $\beta > 0$. Furthermore, to guarantee the existence of an inner horizon r_-, according to (2.4), one must ensure that

$$M > k \Rightarrow \beta < a^2. \tag{2.6}$$

If (2.6) is not satisfied, the spacetime would still describe a rotating black hole but with only one horizon, a geometry whose global structure would be quite different from that of the usual Kerr black hole. We shall therefore restrict our investigation to those black hole geometries which have an inner and outer horizon, that is, focus on values of β satisfying,

$$(a/M)^2 - 1 \leq \beta/M^2 < (a/M)^2. \tag{2.7}$$

[2]The reader should note that our convention is different from [112–114]. In their notation, $\Delta = r^2 + a^2 - 2Mr + \beta$. So, in their case, a positive value of β corresponds to the KN black hole.

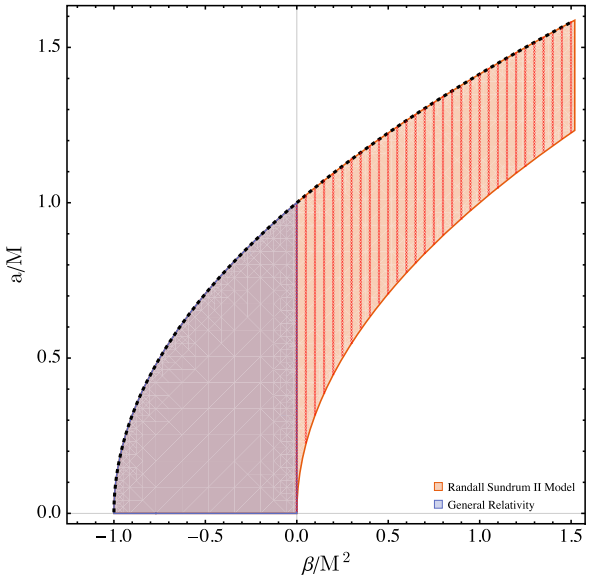

FIG. 1. The space of values of BH spin a and tidal charge β which ensure that the rotating braneworld black hole possesses two horizons is shown in orange. The blue region shows the allowed values of a and β in the Kerr-Newman spacetime provided $\beta = -Q^2$ is interpreted as the usual electric charge. Although the two solutions are fundamentally different, the braneworld BH being a vacuum solution, they are operationally indistinguishable in the region of overlap ($\beta < 0$). The red crosses in the parameter space indicate values of a and β sampled to compute the quasinormal modes in the text, and extremal values of a and β lie on the thick dotted black curve.

In Fig. 1, we have shown the portion of the parameter space spanned by the allowed values a and β in the RS-II braneworld scenario [keeping in mind (2.7)], and compared it with the region described by the KN solution in general relativity. Note that a and β are theoretically unbounded from above. We have also indicated the values of a and β which satisfy the equality in (2.5) by a thick dotted black curve. We term this as the *extremal curve*, and later on we shall call the modes corresponding to a and β lying close to this curve as near-extremal modes. It is evident that the braneworld black hole provides us with an opportunity to explore a much larger portion of the parameter space compared to GR and hence allows us to investigate the imprint of an otherwise hidden extra dimension on various physical phenomena in the strong field regime.

III. MASSIVE SCALAR PERTURBATIONS AROUND THE ROTATING BRANEWORLD BACKGROUND

The goal of the present work is to study the behavior of (massive) scalar field perturbations propagating in the rotating braneworld BH background. Since the seminal work of Vishveshwara [165], quasinormal modes (QNMs), or the characteristic frequencies, of black holes have become ubiquitous to BH physics [166,167]. These modes are triggered by the presence of perturbing fields near the vicinity of the black hole, or due to perturbations to the background metric itself. They carry unique fingerprints of black hole parameters and spacetime geometry, remaining independent of the initial perturbation. While gravitational perturbations are pivotal from an observational standpoint, the study of massive scalar perturbations is important in its own right [42,168]. Setting aside the fact that studying the quasinormal mode spectrum of fields of different spins is the first step toward assessing the stability of the BH, massive scalar fields can act as a useful proxy for more realistic baryonic fields. Hence, they act as a useful precursor to full-scale numerical relativity simulations.

Furthermore, in asymptotically flat spacetimes, the presence of the scalar field mass fundamentally alters the behavior of the scattering potential at infinity since it now asymptotes to a constant value. This feature leads to an interesting behavior in certain QNM frequencies which can become arbitrarily long-lived, giving rise to the phenomena called *quasiresonance*. Moreover, the massive scalar field potential is now able to trap certain modes since due to the presence of a mass barrier, the radial effective potential acts as a reflecting surface. Such modes, called quasibound states (QBSs), decay exponentially near infinity (in contrast to QNM, even though they still leak away through the horizon) and can be extremely long-lived. In fact, these modes can further extract mass and angular momentum from a rotating BH through the familiar superradiance mechanism [168] and become *superradiantly unstable* due to successive reflections from the potential barrier, leading to the growth of a scalar condensate outside the BH horizon. Such configurations are similar to the so-called *black hole bombs* [169,170]. In the nonrelativistic limit, these black hole systems carrying a *boson cloud* are also called gravitational atoms since the system loosely resembles that of a hydrogen atom [171–177]. These gravitational atoms can be an invaluable tool when it comes to probing the existence of ultralight bosons beyond the Standard Model of particle physics [171–177]. Recently, a relativistic framework for studying boson clouds has been proposed as well [178].

In this section, we shall review the basics of the wave equation governing massive scalar perturbations and the appropriate boundary conditions to study QNMs and QBSs. The derivation of the concerned equations and boundary condition is operationally identical to that of massive scalar perturbations in the KN background. We therefore only highlight the major steps and results.

A. The wave equation

We start by considering a test field $\psi(t, r, \theta, \phi)$ of mass μ satisfying the Klein-Gordon (KG) equation.

$$\frac{1}{\sqrt{-g}}\partial_\mu(g^{\mu\nu}\sqrt{-g}\partial_\nu\psi) - \mu^2\psi = 0, \tag{3.1}$$

where g is the determinant of the metric given by (2.2), and we assume that the test field does not backreact on the background [166,167].

Since the metric (2.2) possesses Killing vectors ∂_t and ∂_ϕ, the wave equation (3.1) can be solved by the method of separation of variables, using the *ansatz*,

$$\psi(t,r,\theta,\phi) = e^{-i\omega t+im\phi}S_{lm}(\theta)R_{lm}(r), \tag{3.2}$$

where we have introduced the frequency ω and the azimuthal number m which is an integer since $\exp(im\phi)$ must remain unchanged under the transformation $\phi \to \phi + 2\pi$. Using the ansatz (3.2), we can separate out the KG equation (3.1) into two coupled ordinary differential equations (ODEs) satisfied by the angular and the radial eigenfunctions, $S_{lm}(\theta)$ and $R_{lm}(r)$ respectively. We therefore find that $S_{lm}(\theta)$ satisfies,

$$\frac{1}{\sin\theta}\frac{d}{d\theta}\left(\sin\theta\frac{dS_{lm}(\theta)}{d\theta}\right) + \left(a^2(\omega^2-\mu^2)\cos^2\theta - \frac{m^2}{\sin^2\theta} + A_{lm}\right)S_{lm}(\theta) = 0, \tag{3.3}$$

where A_{lm} is the separation constant of the problem, and (3.3) is known as the scalar spheroidal harmonic equation [179]. In general, the separation constant is arbitrary, but it takes a discrete set of values labeled by l, m when we demand that S_{lm} must be regular at the poles located at $\theta = 0$ and $\theta = \pi$. Then, these solutions are called the scalar spheroidal harmonics, and in the limit $a \to 0$, $S_{lm} \to Y_{lm}$ where Y_{lm} denote the familiar spherical harmonics, and $A_{lm} \to l(l+1)$ with $l \geq |m|$ being a nonnegative integer. Therefore, l and m can also be used to label the modes. Note that by introducing a new variable, $u = \cos\theta$ where the range u is $-1 \leq u \leq 1$, (3.3) can be transformed to the following form,

$$(1-u^2)\frac{d^2S_{lm}(u)}{du^2} - 2u\frac{dS_{lm}(u)}{du} + \left(\bar{\Lambda} + \gamma^2 - \gamma^2u^2 - \frac{m^2}{1-u^2}\right)S_{lm}(u) = 0, \tag{3.4}$$

where we have introduced the constants γ and $\bar{\Lambda}$ such that $\gamma = ia\sqrt{\omega^2-\mu^2}$ and $A_{lm} = \gamma^2 + \bar{\Lambda}$. We can also show that the radial eigenfunction $R_{lm}(r)$ satisfies,

$$\Delta\frac{d}{dr}\left(\Delta\frac{dR_{lm}(r)}{dr}\right) + U_{lm}(r)R_{lm}(r) = 0, \tag{3.5}$$

where,

$$U_{lm}(r) = K^2 - \Delta(\lambda_{lm} + r^2\mu^2), \tag{3.6}$$

with $\lambda_{lm} = A_{lm} + a^2\omega^2 - 2am\omega$, $K = \omega(r^2+a^2) - am$ and $\Delta = (r-r_+)(r-r_-)$.

We see that although (3.1) is separable, the two ODEs (3.3) and (3.5) that we have obtained are coupled and therefore to solve the eigenvalue problem, we need to solve the two equations simultaneously to determine the separation constant A_{lm} and the eigenfrequencies ω. Furthermore, we have to also supplement Eqs. (3.3) and (3.5) with suitable boundary conditions (BCs) dictated by the physics of the problem which we shall now discuss.

B. Boundary conditions, quasinormal modes and quasibound states

To determine the appropriate boundary conditions required to study massive scalar perturbations, we introduce the radial function $\bar{R}_{lm} = \sqrt{r^2+a^2}R_{lm}$ and the tortoise coordinate in the usual manner, viz.,

$$dr_* = \frac{r^2+a^2}{\Delta}dr, \tag{3.7}$$

and rewrite the radial equation (3.5) as,

$$\frac{d^2\bar{R}_{lm}}{dr_*^2} + \bar{U}_{lm}\bar{R}_{lm} = 0, \tag{3.8}$$

where,

$$\bar{U}_{lm} = \left(\omega - \frac{am}{r^2+a^2}\right)^2 - \frac{\Delta}{(r^2+a^2)^2}\left(\lambda_{lm} + H(r)\right), \tag{3.9}$$

with,

$$H(r) = r^2\mu^2 + \frac{(r\Delta)'}{r^2+a^2} - \frac{3\Delta r^2}{(r^2+a^2)^2}. \tag{3.10}$$

Here prime denotes a derivative with respect to r, and the resultant equation (3.8) resembles the Schrödinger equation.

Now due to the presence of the event horizon at $r = r_+$, the black hole system is inherently dissipative or nonconservative: waves that fall into the black hole carry energy out of the system and by the virtue of the definition of an event horizon in classical gravity, nothing can emerge from the event horizon as well. Therefore, the scalar waves must satisfy perfectly ingoing boundary conditions at the horizon. To figure out the form of the boundary condition near the horizon, we need to solve (3.8) asymptotically as $r \to r_+$, or $r_* \to -\infty$, such that $\Delta(r_+) \sim 0$, which in turn implies $\bar{U}_{lm} \sim (\omega - \omega_c)^2$ where

$$\omega_c = \frac{am}{r_+^2+a^2}. \tag{3.11}$$

Noting that near r_+, we can write

$$r_* \sim \frac{r_+^2+a^2}{r_+-r_-}\ln(r-r_+),$$

we find that a solution that is purely ingoing at the event horizon in $v = t + r_*$ coordinates is given by,

$$R_{lm}(r \to r_+) \sim e^{-i(\omega-\omega_c)r_*} \sim (r - r_+)^{-i\delta}, \tag{3.12}$$

where,

$$\delta = \frac{(r_+^2 + a^2)\omega - am}{r_+ - r_-}.$$

Now, depending on the boundary condition we choose to impose at $r \to \infty$, we can have different solutions to the eigenvalue problem specified by (3.8). In addition to the purely ingoing BC at r_+, if we demand that the modes are perfectly outgoing at infinity, we would obtain the *quasinormal modes* (QNMs) of the black hole. However, if the boundary condition is such that the modes decay exponentially near infinity, we get the *quasibound states* (QBSs) of the spacetime. Note that as $r \to \infty$, or $r_* \to \infty$, the potential (3.9) reduces to

$$\bar{U}_{lm} \sim \omega^2 - \mu^2 + \mu^2 \frac{(r_+ + r_-)}{r}, \tag{3.13}$$

and hence we can find an asymptotic solution to (3.8) near infinity to obtain [180–182],

$$\begin{aligned} R_{lm}(r \to \infty) &\sim r^{i(r_+ + r_-)\mu^2/2\Omega - 1} e^{i\Omega r_*}, \\ &\sim r^{i\rho - 1} e^{qr}, \end{aligned} \tag{3.14}$$

where,

$$\rho = \left(\frac{2\omega^2 - \mu^2}{2\Omega}\right)(r_+ + r_-), \tag{3.15}$$

$$\Omega = \pm\sqrt{\omega^2 - \mu^2}, \tag{3.16}$$

$$q = i\Omega = \mp\sqrt{\mu^2 - \omega^2}. \tag{3.17}$$

Note that while obtaining (3.14), we have consistently taken into account the contribution from the subleading terms near infinity, this is important to ensure the accuracy of the continued fraction method discussed in the next section [180]. It is also interesting to note that (3.14) enables us to study QNMs and QBSs in a unified manner, based on our choice of the sign of q in (3.17). If $\mathrm{Re}(q) > 0$, then the solution diverges near $r \to \infty$, and it is consistent with purely outgoing boundary conditions at infinity. Hence, $\mathrm{Re}(q) > 0$ is suitable for studying QNMs. On the other hand, the solution exponentially vanishes near infinity for $\mathrm{Re}(q) < 0$, and hence such a choice is suitable for studying QBSs [183,184]. The eigenfrequencies ω that we shall compute are in general complex, that is $\omega = \omega_R + i\omega_I$, unlike the normal mode frequencies of conservative system, and is therefore a hallmark of the dissipative nature of the system due to the loss of energy through the horizon (and also through the infinity for QNMs). The real part of the frequency, $\mathrm{Re}(\omega) \equiv \omega_R$ represents the frequency of oscillation and the imaginary part $\mathrm{Im}(\omega) \equiv \omega_I$ represents the rate of growth or decay of the perturbation. While studying QNMs, for stable perturbations that decay with time, $\mathrm{Im}(\omega) < 0$ and $|\mathrm{Im}(\omega)|$ can be identified with the decay rate. Since we are studying massive scalar field perturbations, the quasibound states may be prone to superradiant instabilities. Such modes are characterized by $\mathrm{Im}(\omega) > 0$, and it represents the rate of growth of the instability. Furthermore, the oscillation frequency of these modes is supposed to satisfy [185–187],

$$0 < \mathrm{Re}(\omega) < \mu, \quad \text{and} \quad 0 < \mathrm{Re}(\omega) < \omega_c. \tag{3.18}$$

The first of the above two conditions ensures that the modes are reflected from the potential barrier at infinity while the second one is the usual condition for superradiance. These two condition together ensure the growth of the superradiant instability and formation of the gravitational atom.

We end this section by noting that the massive scalar field propagating in the Kerr and Kerr Newman background has received a lot of attention over the last ~50 years since the pioneering studies of Damour, Deruelle, and Ruffini [188], Zouros and Eardley [189], and Detweiler [190], and it continues to be an active area of investigation given its rich phenomenology in light of strong field tests of GR; an excellent description of both the history and the physics of the subject can be found in [168]. In recent times, it is worth mentioning that the massless scalar and gravitational QNMs in the KN background were studied in [191]. The QNM spectra of massive scalar fields for Kerr and Kerr Newman black holes were studied in [192,193]. These studies used the method of continued fractions developed by Leaver [194]. Studies focusing on the instability of the massive scalar field, or the gravitational atom, in the Kerr background was carried out in [183,185,195–197], the same for the Kerr Newman black hole was explored in [184,187,198,199]. Similar studies have been carried out for Kerr-like black holes [182] and galactic black holes as well [200]. But before we move on to study the behavior of massive scalar fields in the context of the braneworld scenario, we discuss the numerical method used to obtain our results in the next section.

IV. A NUMERICAL RECIPE FOR LEAVER'S METHOD OF CONTINUED FRACTIONS

Armed with (3.4), (3.5), and the boundary conditions (3.12) and (3.14), we now attempt to numerically determine the QNMs and QBSs of the braneworld BH. We have chosen the method of continued fractions proposed by Leaver [194] to compute QNMs. The method itself was first used by Jaffé to compute the electronic spectra of

hydrogen molecular ion, and over the years it has been widely used to compute the QNMs and QBSs of various black hole geometries. We shall first write down the necessary recurrence relations which resemble those of the KN black hole, and then discuss a strategy based on [182] to scan the parameter space (cf., Fig. 1) in a manner that assures convergence.

A. Radial equation

We begin by considering the following *ansatz* for the radial differential equation that takes into account the BCs (3.12) and (3.14), viz.,

$$R_{lm}(r) = e^{i\Omega r}\left(\frac{r-r_+}{r-r_-}\right)^{i\delta}(r-r_-)^{i\rho}P(r), \tag{4.1}$$

where,

$$P(r) = \sum_{n=0}^{\infty} d_n \left(\frac{r-r_+}{r-r_-}\right)^n.$$

We then plug in (4.1) into (3.5) to obtain a three term recurrence relation satisfied by the coefficients a_n, namely,

$$\alpha_0^r a_1 + \beta_0^r a_0 = 0, \tag{4.2}$$

$$\alpha_n^r d_{n+1} + \beta_n^r d_n + \gamma_n^r d_{n-1} = 0, \qquad n \geq 1 \tag{4.3}$$

with,

$$\alpha_n^r = n^2 + (c_0+1)n + c_0, \tag{4.4a}$$

$$\beta_n^r = -2n^2 + (c_1+2)n + c_3, \tag{4.4b}$$

$$\gamma_n^r = n^2 + (c_2-3)n + c_4 - c_2 + 2, \tag{4.4c}$$

and,

$$c_0 = 1 + \frac{2i}{(r_+-r_-)}\left(am - \omega(a^2+r_+^2)\right), \tag{4.5a}$$

$$c_1 = -2(c_0+1) + 4ir_+\Omega + \frac{i\mu^2(r_++r_-)}{\Omega}, \tag{4.5b}$$

$$c_2 = c_0 + 2 - i(r_++r_-)\left(\frac{2\omega^2-\mu^2}{\Omega}\right), \tag{4.5c}$$

$$c_3 = c_0\left[c_0 + \frac{c_1}{2} + i\omega(r_++r_-)\right] - i\omega(r_++r_-) + a^2\omega^2 + r_+^2(2\omega^2-\mu^2) - A_{lm}, \tag{4.5d}$$

$$c_4 = c_0 - i(r_++r_-)(c_0-1)\omega - \frac{(r_++r_-)^2\mu^4}{4\Omega^2} - i(r_++r_-)(c_0+1)\frac{(2\omega^2-\mu^2)}{2\Omega}. \tag{4.5e}$$

We now divide the (4.3) by d_n and then, after a minor rearrangement, obtain

$$\frac{d_n}{d_{n-1}} = -\frac{\gamma_n^r}{\beta_n^r + \alpha_n^r \frac{d_{n+1}}{d_n}}. \tag{4.6}$$

Now (4.6) can be cast in the form of an infinite continued fraction by substituting the expression for d_{n+1}/d_n [obtained by replacing n with $n+1$ in (4.6)] back into (4.6), and iterating the process till we obtain,

$$\frac{d_n^r}{d_{n-1}^r} = -\cfrac{\gamma_n^r}{\beta_n^r - \alpha_n^r \cfrac{\gamma_{n+1}^r}{\beta_{n+1}^r - \alpha_{n+1}^r \cfrac{\gamma_{n+2}^r}{\beta_{n+2}^r - \cdots}}}. \tag{4.7}$$

Putting $n=1$ in (4.7) and equating it with (4.2) we further get,

$$0 = \beta_0^r - \frac{\alpha_0^r\gamma_1^r}{\beta_1^r-}\frac{\alpha_1^r\gamma_2^r}{\beta_2^r-}\cdots\frac{\alpha_n^r\gamma_{n+1}^r}{\beta_{n+1}^r-}\cdots. \tag{4.8}$$

The above continued fraction can be inverted n number of times to yield,

$$\beta_n^r - \frac{\alpha_n^r\gamma_{n+1}^r}{\beta_{n+1}^r-}\frac{\alpha_{n+1}^r\gamma_{n+2}^r}{\beta_{n+2}^r-}\cdots = \frac{\alpha_{n-1}^r\gamma_n^r}{\beta_{n-1}^r-}\cdots\frac{\alpha_0^r\gamma_1^r}{\beta_0^r}. \tag{4.9}$$

We note that putting $n=0$ in (4.9) gives back (4.8), provided that for $n<0$, $\alpha_n = \beta_n = \gamma_n = 0$. If we know the value of the separation constant A_{lm} appearing Eq. (4.5d), we can truncate the continued fraction at a suitably large value N and solve the algebraic equation using an appropriate root finding algorithm to determine the QNM or QBS frequency ω depending on the sign of Ω (as discussed in the previous section), thereby solving the radial eigenvalue problem. The infinite continued fraction (4.9) in principle has an infinite number of roots, however numerically, the nth inversion gives the nth stable root. So to study the fundamental mode, we have to put $n=0$ in (4.9). The inverse continued fraction is actually more useful in calculating the overtones.

Since we truncate the continued fraction at some N, the *remainder* of the series $R_N = -d_{N+1}/d_N$ can be approximated following Nollert's prescription [201]. Since R_N satisfies the recurrence relation,

$$R_N = -\frac{\gamma_{N+1}^r}{\beta_{N+1}^r - \alpha_{N+1}^r R_{N+1}}, \tag{4.10}$$

we can then expand R_N as a power series, viz.,

$$R_N = \sum_{k=0}^{\infty} C_k N^{-k/2},$$

and then by equating the coefficients of each power of $\sqrt{N}$ to zero, we obtain the first three coefficients as,

$$C_0 = -1,$$
$$C_1 = \pm\sqrt{-2i\Omega(r_+ - r_-)},$$
$$C_2 = \frac{3}{4} + 2i\Omega r_+ + \frac{i\mu^2(r_+ + r_-)}{2\Omega}.$$

Note that the sign of C_1 is chosen in such a way that $\mathrm{Re}(C_1)$ should be positive to ensure convergence. Now for a large value of N, the contribution from the terms following N become very small. So, including terms beyond the N^{th} term should not significantly alter the value of the root the continued fraction. However, rather than simply discarding or selecting an arbitrary value for the remaining part, it is preferable to apply Nollert's prescription since Nollert observed that it is crucial when one attempts to calculate modes whose imaginary parts are much larger than their real part, and as a result improves the overall convergence of Leaver's method.

B. Angular equation

We need to solve the angular equation (3.4) to determine the separation constant A_{lm} by imposing the boundary condition that the function $S_{lm}(u)$ is regular at the poles $u = \pm 1$. Taking this into consideration, the series solution for the angular wave-function takes the form,

$$S_{lm} = e^{i\Omega u}(1+u)^{m/2}(1-u)^{m/2}\sum_{n=0}^{\infty} c_n(1+u)^n, \quad (4.11)$$

Substituting (4.11) into (3.4) yields the following three term recurrence relation

$$\alpha_n^\theta c_{n+1} + \beta_n^\theta c_n + \gamma_n^\theta c_{n-1} = 0, \quad (4.12)$$

where

$$\alpha_n^\theta = 2(n+1)(n+m+1), \quad (4.13a)$$

$$\beta_n^\theta = -n^2 + n(4a\Omega - 2m - 1) + A_{lm} + a^2\Omega^2 + (2a\Omega - m)(m+1), \quad (4.13b)$$

$$\gamma_n^\theta = -2a\Omega(n+m). \quad (4.13c)$$

Although we can solve both the radial and angular equations on an equal footing using Leaver's method, in practice we have found that it often much more computationally inexpensive to use a suitable library function [200] to compute A_{lm}.

C. Implementation

Since we have transformed the problem of finding out the eigenvalues of the ODEs (3.4) and (3.5) into a problem of finding the roots of an infinite continued fraction (4.9), we can solve (4.9) to determine the eigenfrequency ω by specifying the set of values $B = \{a, \beta, \mu, l, m\}$ along with the number of terms to include in the continued fraction N and a suitable guess value ω_0 for the root-finding algorithm. To use (4.9), we also need to specify n, the number of inversions of the continued fraction (4.8), and since we shall be focusing on the fundamental mode, we set $n = 0$. We also set $M = 1$ as the characteristic length scale which means that all dimensionful quantities are suitably scaled with respect to M and made dimensionless.

To ensure convergence of the mode $\omega(B)$ for a set of values specified by B and ω_0, we adopt the following strategy: we first determine $\omega(B)$ for $N = N_1$, and then increment N by dN and recompute the value of $\omega(B)$. We continue the iteration until N reaches a maximum value $N_{\max}$, or the relative difference between the values of $\omega(B)$ from two successive iterations falls below a specified tolerance $\epsilon = 10^{-p}$. Symbolically, if $\omega(B;N)$ is the value of the root $\omega(B)$ obtained by keeping N terms in the continued fraction, we break the iteration when

$$\log_{10}\left|1 - \frac{\omega(B;N+dN)}{\omega(B;N)}\right| < -p. \quad (4.14)$$

In our calculation, we have set $p = 7$, ensuring that our results converge up to at least six decimal places, unless stated otherwise. The values of $\{N_1, dN, N_{\max}\}$ are so chosen as to ensure that the computation finishes in a feasible amount of time on a workstation while ensuring convergence, e.g.: for the $l = m = 0$ QNMs, we take, $N_1 = 100, dN = 100, N_{\max} = 5000$. We have also noticed that while computing QNMs, the continued fraction converges for relative small values of $N \sim 300$–600 when the black hole is far from extremality, but for near-extreme configurations it requires a high value of $N \sim 1000$–3000 on average to ensure that the modes converge to six decimal places. Since the scattering problem in black hole spacetimes is inherently dissipative, the eigenvalue spectrum is prone to numerical instabilities arising from rounding-off errors due to machine precision arithmetic [202], therefore it is customary and prudent to perform intermediate calculations using extended precision. In our work we have therefore set the internal precision to at least $4 \times$ MachinePrecision. The strategy outlined so far is used in the computation of both the QNMs and QBSs.

In order to determine the quasinormal modes, we scan the parameter space Fig. 1 in the following manner: we fix the values of l, m and the mass μ of the scalar field and choose a value of the tidal charge β. Since there is theoretically no restriction on the value of the tidal charge, we restrict ourselves to $\beta \leq \beta_{\max} = 1.5$. We then increment

the value of a from 0 to the maximum possible value $a_{\max} = \sqrt{1+\beta_{\max}}$ in steps of $da = 0.01$, and calculate the corresponding fundamental QNM frequency ω for those values of a given β such that the inequality given by (2.7) is satisfied. For the first allowed value of a given β, we use a value approximately equal to the of the fundamental massless scalar quasinormal mode of a Schwarzschild BH or a slowly rotating Kerr BH ($a = 0.000001$) as the initial guess value ω_0 for the root-finding algorithm.[3] But for subsequent iterations, we use the value of the mode found in the previous iteration as the new value of ω_0. This is advantageous because near extremality, we found that the convergence of the root-finding algorithm is extremely sensitive to the choice of ω_0; for an "improper" choice of ω_0, the algorithm may also return a value of ω that corresponds to an overtone instead of the fundamental mode. We repeat the process described so far for other values of β in parallel, and we choose values of β lying between 0 and $\beta_{\max}$ in steps of $d\beta = 0.05$. The sampled points are shown in Fig. 1 as red crosses.

To compute the quasibound states and the associated superradiant instability, we follow a slightly modified approach to scan the parameter space Fig. 1 since the root finding algorithm is extremely sensitive to choice of guess values for nonzero values of β and μ. We proceed in two major steps. First, we fix the values of l, m, and μ and then, by using a guess value ω_0 [based on (3.18)] such that its real and imaginary parts are $\mathrm{Re}(\omega_0) = 0.95\mu$ and $\mathrm{Im}(\omega_0) = 10^{-8}$ respectively, we calculate the QBSs for $a \sim 0$ and $\beta = 0$. We now keep $a \sim 0$ fixed and increase the value of β by $d\beta = 0.01$. Then, using the value of the mode we have just computed as the new guess value, we compute the QBS for $a \sim 0$ and $\beta = d\beta$. We then move horizontally by incrementing β until we reach $\beta_{\max} = 1.5$, keeping $a \sim 0$ fixed all the while. This step gives us the first rung of guess values that we shall use in the second major step to scan the parameter space by moving vertically upward, that is, by keeping β fixed and incrementing a by $da = 0.01$ for each β in parallel. In subsequent iterations, we shall use the mode computed in the previous step as new guess value. This process is different from the one employed in computing QNMs in two ways: first, we use a "customized" guess value for each β and second, we end up computing the QBSs even for those geometries for which $\beta > a^2$. However, while plotting the results we discard those values of a and β that violate the inequality given by (2.7).

We are also interested in how the modes behave with respect to variations in μ, focusing on a much smaller set of values of a and β. So, now we fix the values of a, l, m, and choose a set of values of β which satisfies (2.7). Then for each pair of a and β, we calculate the quasibound state starting with $\mu = \mu_{\min}$. We then increment μ in steps of $\mathrm{d}\mu$ up to $\mu_{\max}$. For the first iteration, while calculating the QBS for $\mu_{\min}$, we set the real and imaginary part of the guess value to $\mathrm{Re}(\omega_0) = 0.95\mu_{\min}$ and $\mathrm{Im}(\omega_0) = 10^{-8}$ respectively, in accordance with (3.18). In subsequent iterations, we use the value of the QBS computed in the previous step as the new guess value. For quasibound states, the first overtone tends to lie very close to the fundamental mode, and hence the root-finding algorithm might be highly sensitive to the choice of the guess value. In our approach, this difficulty may be ameliorated by choosing a smaller value of $d\mu$. Furthermore, in the regime of the superradiant instability, the imaginary part of the QBS has a very small positive value compare to its real part. Therefore, to ensure that the modes do indeed converge, we have to apply the criteria given by (4.14) to both real and imaginary parts of ω separately and simultaneously. We have observed that the real part converges much faster than the imaginary part and hence requires a stricter test.

Lastly, we have validated our approach by confirming that it is able to reproduce existing results related to the quasinormal modes and quasibound states of Kerr and Kerr-Newman black holes [183,184,200].

V. NUMERICAL RESULTS

In this section, we shall present the results of our numerical explorations, focusing first on the quasinormal modes, and then on the quasibound states and the associated superradiant instability.

A. Quasinormal mode spectra

The fundamental quasinormal modes of the rotating braneworld black hole has been show in Fig. 2 for various (normalized) values of the tidal charge β, BH spin a, and scalar field mass μ, each subfigure corresponding to different values of l and m. Each curve in the complex plane is labeled by β, and the color of each point corresponds to the value of a, whereas the value of μ is indicated by the shape of the marker. In Fig. 2, we have restricted ourselves to $0 \leq \beta \leq 1$, with the value of a being constrained by (2.7). However, theoretically there is no upper bound on β. Hence, we have also explored the $\beta > 1$ regime as well, and to get an idea of how the QNMs behave for different values of β, a, μ, we have presented contour plots showing how the real and imaginary part of the QNMs vary with respect to a and β for massless and massive

[3]The initial guess value, or an approximate value of the fundamental mode of the Schwarzschild or the slowly rotating Kerr black hole can itself be estimated by computing the logarithm of the absolute value of right-hand side of (4.8) over a suitable region of the complex plane, and checking for which value of $\omega = x + iy$, we get a minimum, since this point will lie close to the root of the continued fraction that we are after. The process can be repeated for two values of N to ensure that the minima is not a numerical artifact.

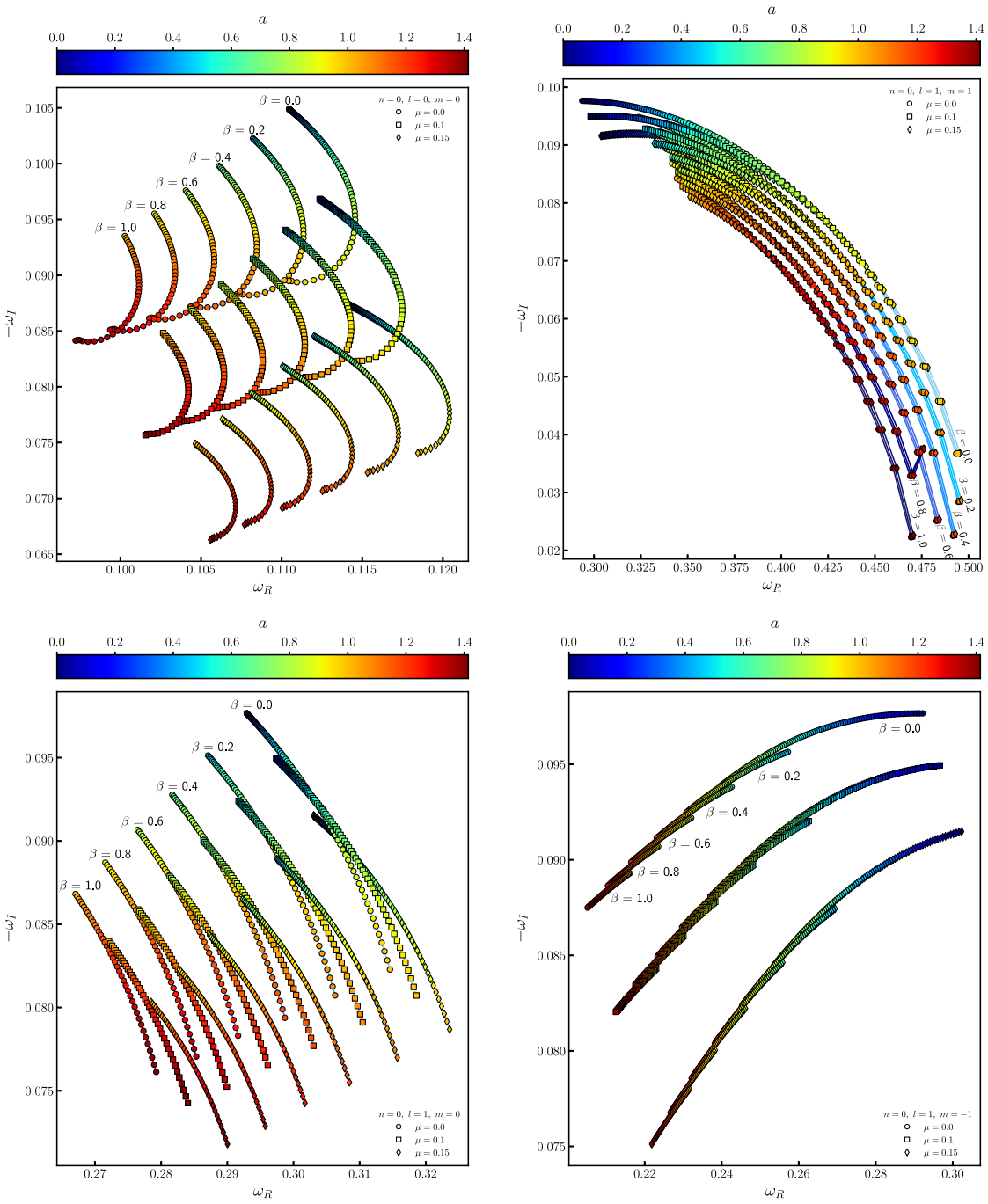

FIG. 2. The quasinormal mode spectra of the rotating braneworld black hole for $l = m = 0$ (top left), $l = m = 1$ (top right), $l = 1$, $m = 0$ (bottom left) and $l = 1, m = -1$ (bottom right). Each curve in the complex plane is labeled by β, and the color of each point corresponds to the value of a, whereas the value of μ is indicated by the shape of the marker. In these figures, we have set the characteristic length scale given by the black hole mass M to unity.

perturbations in Fig. 3, and in Figs. 5 and 6 for $l = 0, 1$ respectively.

For QNMs, recall that $\mathrm{Re}(\omega)$ represents the frequency of oscillation and $|\mathrm{Im}(\omega)|$ stands for the rate of decay of the perturbations. For the $l = m = 0$ modes, we observe from the top left panel of Fig. 2 that if we fix β, then the frequency of oscillation increases with a until it reaches its maximum value. After reaching the maximum, the frequency of oscillation decreases with further increase in a, while the decay rate becomes nearly constant as the black hole approaches extremality.

From the top left panel of Fig. 2, we can also see that when the mass μ of scalar field is turned on, the modes move closer to the real axis. However, in the presence of

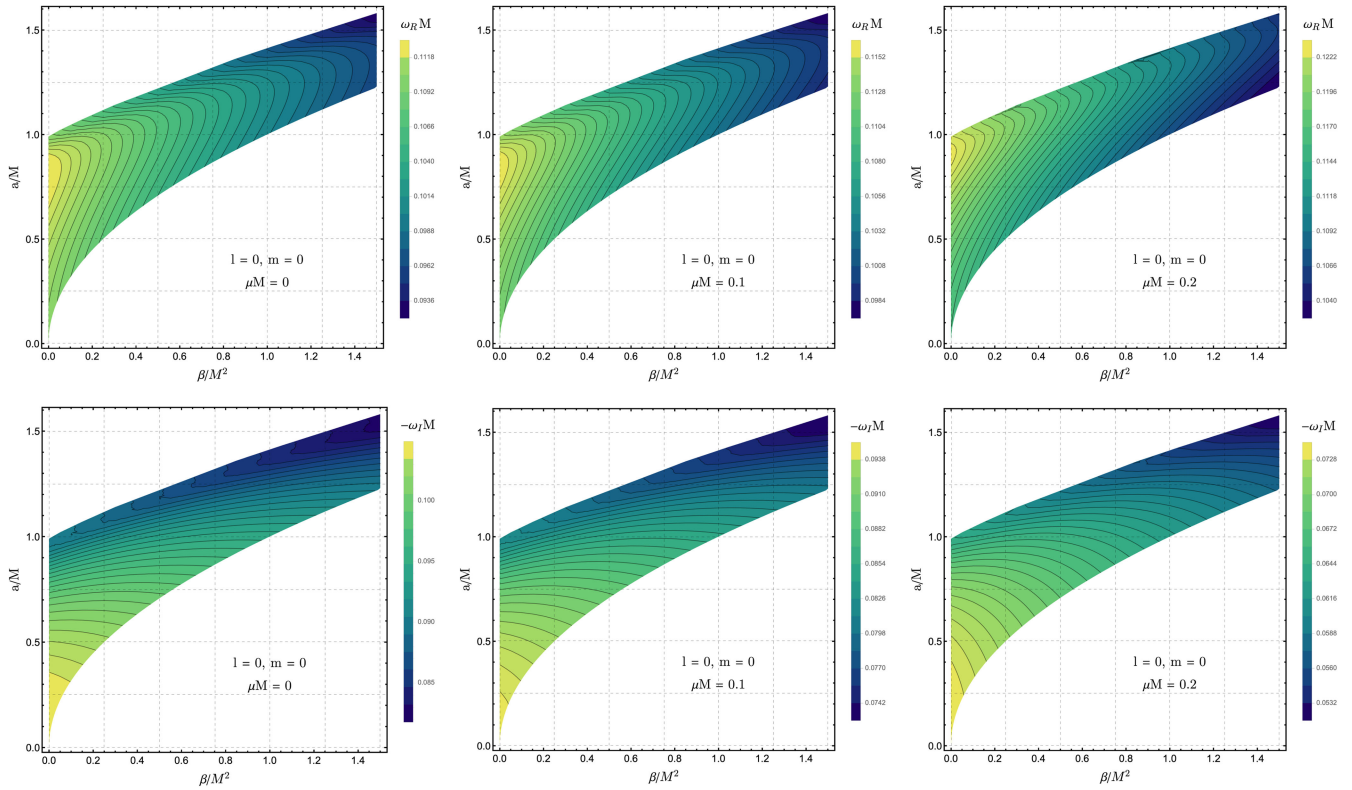

FIG. 3. The real (top row) and imaginary (bottom row) parts of the scalar quasinormal mode spectra corresponding to the $l = m = 0$ mode for $\mu M = 0$ (left column), $\mu M = 0.1$ (middle column), $\mu M = 0.2$ (right column) for the allowed values of a/M and β/M^2.

μ, the change in the decay rate $\mathrm{Im}(\omega)$ is much more pronounced than that in the frequency of oscillation $\mathrm{Re}(\omega)$. In fact, if we keep β and a fixed, and gradually increase μ, then the imaginary part of the QNM will increasingly tend to a value very close to zero. Since these modes will have a finite $\mathrm{Re}(\omega)$ and an extremely small but negative $\mathrm{Im}(\omega)$, these modes will be arbitrarily long-lived. Such modes are called *quasiresonance modes* [90,180,183,203–213], and they satisfy the QNM boundary conditions. They exist even for near extremal configurations, and we explicitly demonstrate the same in Fig. 4.

The contour lines in the top panel of Fig. 3 indicate that the $l = m = 0$ modes with the largest oscillation frequency occur for smaller values of the tidal charge (that is, toward the left of the parameter space under consideration) and from the bottom panel of the same figure, we can see that these modes are also associated with a higher decay rate indicating that they are the least long-lived modes. We also see that the oscillation frequency is maximum when the two horizons of the BH are moderately separated but when the scalar field acquires mass, the maximum begins to shift toward extremal configurations. It is also evident from the bottom panel of Fig. 3 that the decay rate of perturbations in extremal configurations are smaller and hence they are more long-lived than their subextremal counterparts. Turning on μ, we can see (from scales on the color bars) the corresponding decay rates become smaller. Lastly, we observe that the long-lived modes lie in the upper-right region of the parameter space for both the massless and massive cases, that is, in the regime of high values of both β and a, and the corresponding modes have the lowest frequency of oscillation.

Next we consider $l = 1$ modes, and we notice in Fig. 2 that the behavior of the modes varies with azimuthal number $m = -1, 0, 1$. It is evident from Fig. 2 that all the $l = 1$ modes have a higher frequency of oscillation compared to the $l = 0$ modes for all the β and a values that have been considered. Notice that for the $m = 0, 1$ modes (bottom left and top right panels respectively), if we keep β fixed and increase a, then the frequency of oscillation increases whereas for $m = -1$ modes (bottom right panel), it decreases. The decay rates for all m values decrease if a is increased while keeping β fixed.

Let us first look closely at the $l = 1, m = -1$ modes: in the extreme left panel of Fig. 5, we see the modes with the smallest frequency of oscillation occur for larger values of both β and a as they tend to cluster on the upper right side of the parameter space, and from Fig. 6, it is evident that these modes also have the smallest decay rates; the longest-lived modes therefore occur for smaller values β and a. The inclusion of μ does not change the qualitative behavior of the modes even though they tend to reduce the values of both the oscillation frequency and decay rate. In fact, from

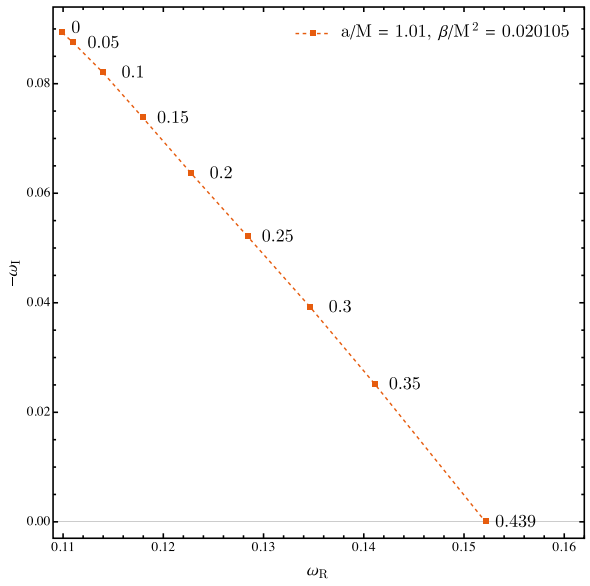

FIG. 4. The formation of quasiresonance state in a near-extremal rotating braneworld black hole spacetime for $l=m=0$ and $a/M>1$ with $\beta>0$, such that $r_{-}=0.995538r_{+}$. The labels alongside the points indicate the value of the scalar field mass μM.

the bottom right panel of Fig. 2, it is clear that the change in the decay rate is much more drastic in the presence of μ compared to the change in the oscillation frequency. Moreover, for sufficiently large values of β and μ one could possibly obtain quasiresonance modes near extremality.

Now, based on the middle panels of Figs. 5 and 6, we observed that the $l=1$, $m=0$ modes with the smallest frequency of oscillation occurs for large values of β but smaller values a. But the near-extremal modes (especially those occurring near the top right corner of the parameter space) are the ones with the smallest decay rates, and hence they are longest-lived modes. The aforementioned figures along with the bottom left panel of Fig. 2 also show that the presence of the mass μ increases the oscillation frequency of these modes but at the same time makes the modes long-lived by significantly decreasing the decay rate. In fact, for large enough values of β and μ, quasiresonance could be achieved by these modes as well.

Let us finally talk about the $l=m=1$ modes in detail: from the extreme right panel of Fig. 5, we see that oscillation frequencies of both massless and massive perturbations are higher for black holes near extremality, and since the contours are nearly parallel to the extremal

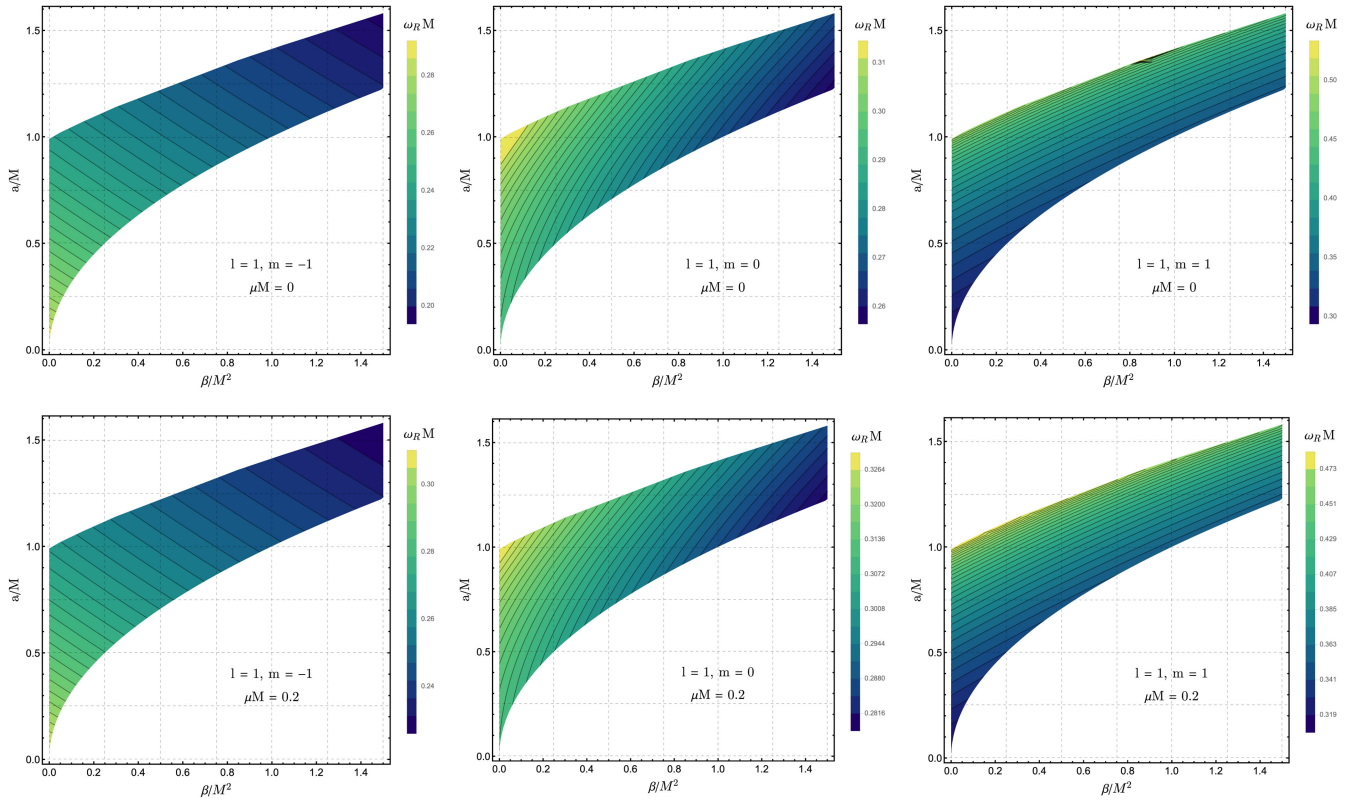

FIG. 5. The real part of the scalar quasinormal mode spectra corresponding to $l=1$ and $m=-1$ (left column), $m=0$ (middle column), $m=1$ (right column) for the allowed values of a/M and β/M^2 for $\mu M=0$ (top row) and $\mu M=0.2$ (bottom row).

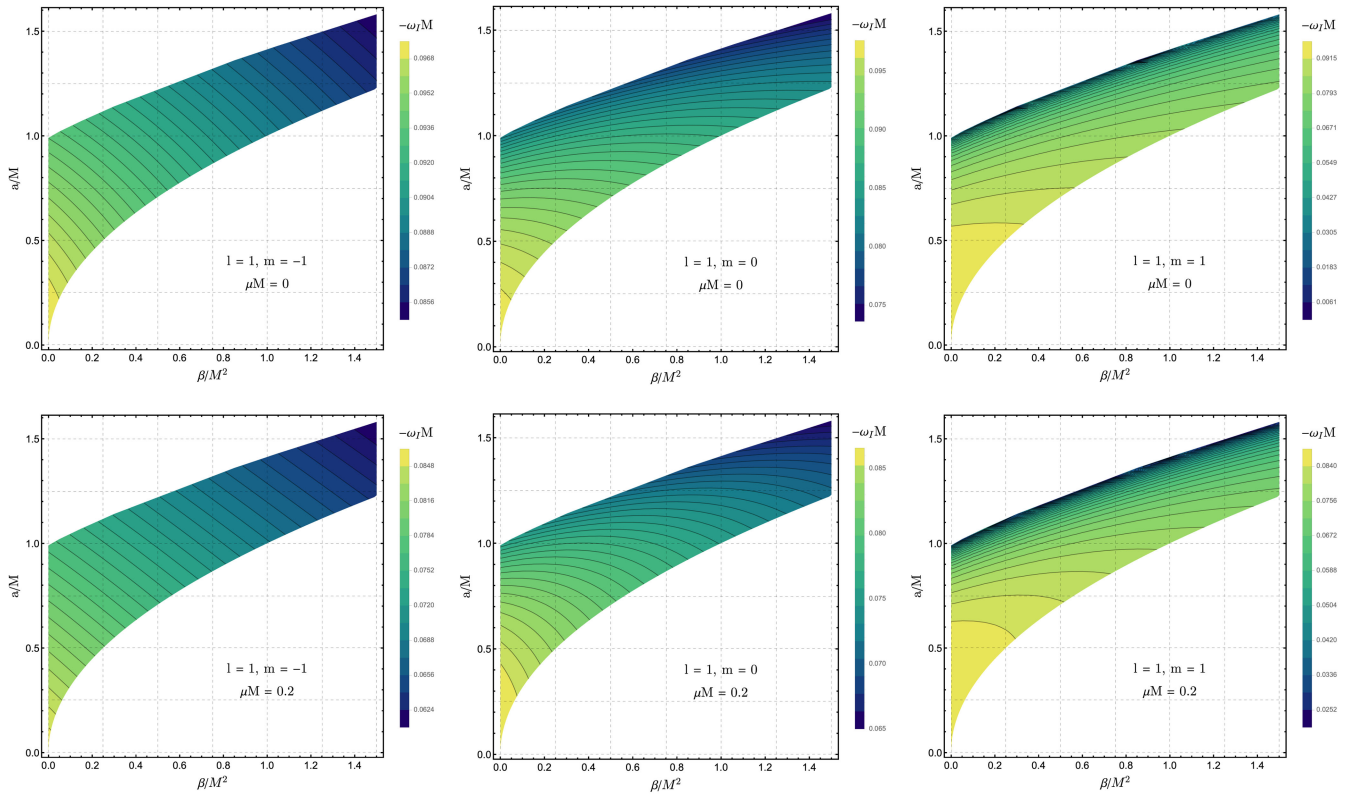

FIG. 6. The imaginary part of the scalar quasinormal mode spectra corresponding to $l = 1$ and $m = -1$ (left column), $m = 0$ (middle column), $m = 1$ (right column) for the allowed values of a/M and β/M^2 for $\mu M = 0$ (top row) and $\mu M = 0.2$ (bottom row).

curve, it indicates that they approach a constant value. The smallest values of both a and β corresponds to modes with the smallest oscillation frequencies. When it comes to the decay rates, from the extreme right panel of Fig. 6, it is clear that the near-extremal modes have the smallest decay rates and hence they are extremely long-lived. In fact, for massless perturbations, they may be extremely close to zero. This feature can also be extrapolated from the trajectories in the complex plane as shown in the top right panel of Fig. 2, and it points toward the existence of the well-known zero damped modes (ZDMs) [193,214,215]. The ZDMs of near extreme and extreme Kerr and KN family of BHs have been extensively studied in the past, and they are quite distinct from the phenomenon of quasiresonance mentioned earlier. The quasiresonance modes are arbitrarily long-lived and have a very small imaginary part: they are associated only with the presence of massive fields whereas ZDMs can occur only for certain values of m for massless perturbations. Now the mass of the scalar field has an intriguing effect on the behavior of the modes: from Fig. 2 we see that for smaller values of β and a, increasing μ enhances the oscillation frequency slightly and reduces the decay rate but the effect is completely washed out as one approaches extremality. Notice how the modes corresponding to different values of μ clump together as one increases a while keeping β fixed in the top right panel of Fig. 2. It seems likely that near extremality, the quasiresonance frequencies approach those of the ZDMs. However, the interplay between ZDMs and quasiresonance modes needs to be probed further numerically to arrive at a definite conclusion. We wish to return to such questions in the future.

At this juncture, it would be pertinent to briefly review some of the previous studies related to the quasinormal mode spectra of braneworld black holes and put our present work in its proper context. Notably, massless scalar and gravitational QNMs were studied in [137,138] for the spherically symmetric case. In [139], the authors studied massive scalar and Dirac perturbations in a mutated Reissner-Nordström black hole which is degenerate to the spherically symmetric braneworld solution found in [111]. In the parameter space shown in Fig. 1, these solutions lie along the x axis and have not been considered in the present study as we have focused on rotating solutions with two horizons.

The gravitational QNM spectrum for the rotating braneworld BH has been investigated in [140] where the authors focused on the $l = m = 2, 3$ modes. They had considered rotating BHs with both single and double horizons. It is interesting to ask how the behavior of the gravitational modes compare to the scalar modes studied here. However, such a comparison is restricted by the fact that while

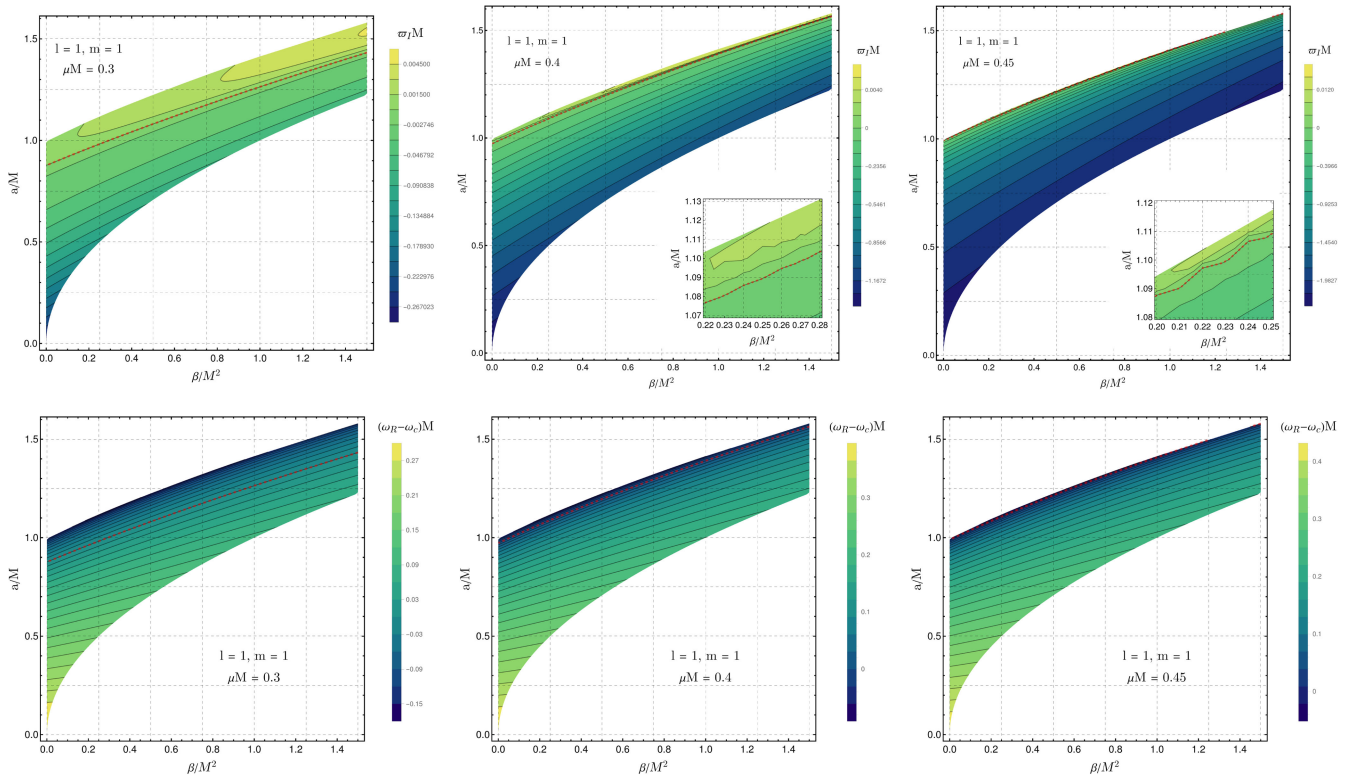

FIG. 7. The imaginary part (top row) of the fundamental quasibound state frequency and the difference between the corresponding real part and $\omega_c = am/(r_+^2 + a^2)$ (bottom row) for the $l = m = 1$ massive scalar perturbations of mass $\mu M = 0.3$ (left column), 0.4 (middle column), and 0.45 (right column) of the rotating braneworld black hole. The red dashed curve represents the zero contour line.

analyzing gravitational perturbations, one has to implement an approximation to separate the wave equation. Such an approximation is similar in spirit to the one employed in the Kerr-Newman case, and it restricts one to small values of β and a [191]. For (massive) scalar perturbations, we do not have to employ any approximation to separate the wave equation, and hence we are allowed to explore the entire length and breadth of the parameter space.

In the restricted portion of the parameter space explored in [140], it was reported that for a particular value of β, if one increases a, the frequency of oscillation increases while the rate of decay decreases for the $l = m = 2, 3$ gravitational mode. They further reported that the change in the decay rate in such a situation was smaller compared to the change in the oscillation frequency. Our study confirms that a similar behavior is exhibited by the $l = m = 1$ modes. They have also highlighted that for a fixed value of a, with an increase in the value of the tidal charge β, both the real and imaginary part of the $l = m = 2, 3$ gravitational QNM decreases. The $l = m = 1$ scalar perturbations show a similar behavior for small values of a, but the behavior is not monotonically decreasing when one consider larger values of a. Moreover, in this case as well, the change in the imaginary part of the QNM frequency is smaller than the corresponding change in the real part. We also note that in [141], the authors tried to constrain the value of the tidal charge using gravitational wave data. But it seems that current observations are unable to strongly discriminate between GR and the braneworld scenario.

Lastly, we end this section with the null result that we could not to find any mode with $\mathrm{Im}(\omega) > 0$ (in the region of the parameter space explored in this work) which points toward the stability of the rotating braneworld black hole as far as QNMs are concerned.

B. Quasibound states and superradiant instability

We now focus on the effect of the tidal charge on the quasibound states (QBSs) and the associated superradiant instability. For massive scalar fields around the Kerr BH, the most unstable modes are those corresponding to $l = m = 1$ and $n = 0$ and the maximum superradiant instability occurs for a near extreme Kerr BH when the mass of the scalar field is $\mu M \sim 0.42$ [183]. Furthermore, taking a hint from the rich structure of the QBS spectrum of the KN black hole [184], we shall also restrict ourselves to the $l = m = 1$ and $n = 0$ modes, and first study the quasibound states for three representative values of the scalar field mass, viz., $\mu M = 0.3$, 0.4, 0.45 over the entire parameter space, the result of which has been shown in Fig. 7. We shall then explore the superradiant instability for smaller set of values of a and β, as shown in Figs. 8–11.

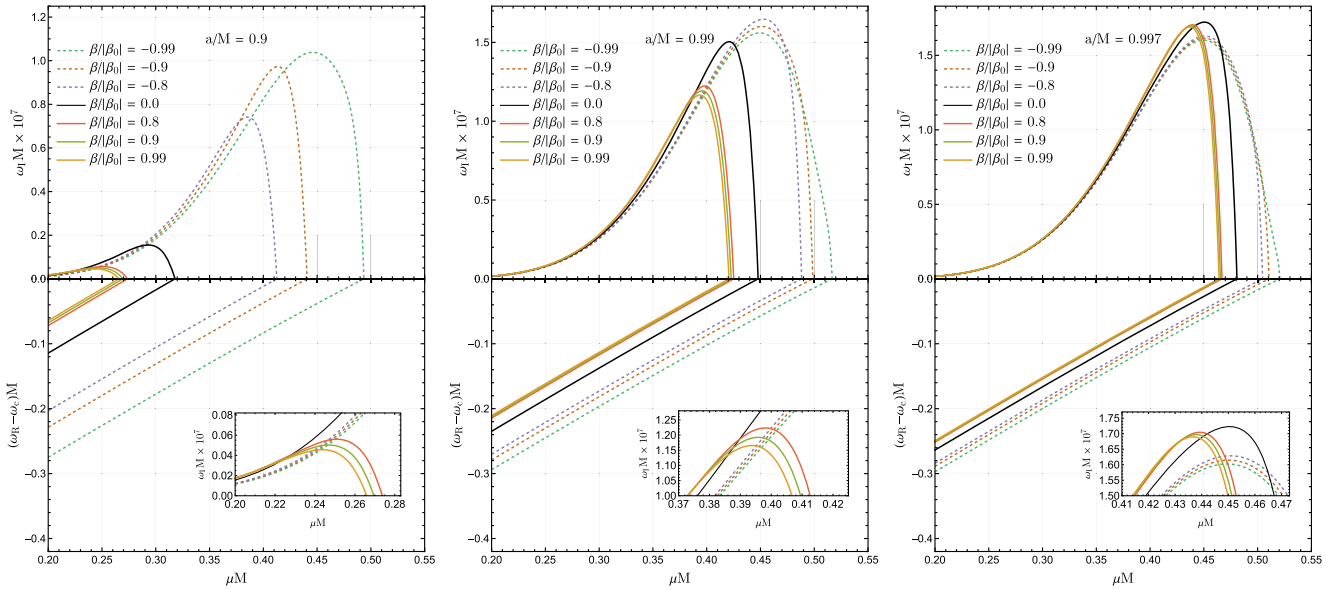

FIG. 8. The superradiant instability associated with the quasibound state spectrum of a massive neutral scalar field ($l = m = 1$) for different values of BH spin $a/M < 1$ and tidal charge β.

Before proceeding, we note that the effect of the tidal charge on superradiance was recently studied in [142] by analyzing the amplification factors of massless scalar waves being scattered by the black hole. However, for massive scalar fields, the analysis has been limited to analytical examinations of extremal configurations [143] where some interesting bounds were obtained on the tidal charge and the BH parameters that ensured that the configuration is superradiantly stable. But a complete numerical analysis of quasibound states and superradiant instabilities of rotating braneworld black hole spanning the entire parameter space has been lacking, and the analysis presented in this section aims to address this gap in the literature.

In Fig. 7, the top row shows the imaginary part of the QBS frequency and the bottom row shows the difference between the corresponding real part and ω_c [cf. (3.11)] for three representative values of μM. The bottom row helps us understand where the superradiance condition given by (3.18) is satisfied. Now, the spectrum of quasibound states contain frequencies whose imaginary parts can be positive, negative, or zero. Furthermore, modes that have a positive imaginary part can be very small and are of the order 10^{-7} for the Kerr BH [183]. So in order to visualize these modes, we use a "symmetric log" scale, that is, we scaled the imaginary part of the frequency ω_I as

$$\varpi_I = \mathrm{Sgn}(\bar{\omega}_I)\big(\log_{10}(|\bar{\omega}_I M| + 1)\big),$$

where $\bar{\omega}_I = \mathrm{Im}(\omega) \times 10^5$ and Sgn denotes the signum function. Also, in Fig. 7, the red dashed curve corresponds to the zero contour line. From the left column of Fig. 7, we see that for $\mu M = 0.3$, the quasibound states with the largest growth rate ($\mathrm{Im}(\omega \mathrm{M}) > 0$) occurs at the upper right region of the parameter space and hence, is associated with large values of β and a. These modes also satisfy the superradiance condition. The modes lying on the zero contour indicated by the red dashed line are particularly interesting because they correspond to bound states whose frequencies are purely real with $\mathrm{Re}(\omega) = \omega_c$. The QBSs lying below the zero contour are damped, and the rate of decay increases with the simultaneous decrease of a and β. Moreover, as the damping increases, the frequency of oscillation increases as well. If we now keep increasing the mass of the scalar field, μM, the growing modes tend to occur nearer and nearer to the extremal curve (2.5) as evident from the middle and right columns of Fig. 7, and eventually the growing modes will disappear. It is also important to note that the maximum instability for positive values of β is of the order of 10^{-7}, and hence comparable to the Kerr case [183].

One can also see that contour lines lying in the region above the zero contour in the top left panel of Fig. 7 are rather curved compared to the ones lying in the region below. This feature suggests that the BH parameters and μ together determine the maximum superradiant instability in a rather nontrivial manner. But since Fig. 7 shows how drastically the region above the zero contour shrinks as one increases μM and how the zero contour remains roughly parallel to the extremal curve, focusing on a small set of values of a and β near $a/M = 1$ is enough to establish the order of the maximum superradiant instability in braneworld black hole. In other words, in the region of the parameter space that we have considered so far, since the contour plots in Fig. 7 already indicate that the maximum superradiant instability is comparable to that of the Kerr BH

and tends to occur near the extremal curve as we progressively increase μM, we can then focus on a set of values of a and β lying around $a/M = 1$, without loss of generality, to estimate which values of μM can trigger the maximum instability for a set of BH parameters. Such an approach would be perhaps more economical than scanning the entire parameter space for the maximum instability [182].

So, first let us focus on the case when $a/M < 1$. The results are summarized in Fig. 8 where we have considered three values of the rotation parameter, $a = 0.9M, 0.99M, 0.997M$. For each value of a we have considered a set of values of tidal charge β normalized by the absolute minimum value of β, that is, $\beta_0/M^2 = |(a/M)^2 - 1|$ [cf., (2.5)] in order to aid comparison across the a values. Furthermore, the dashed curves in Fig. 8 correspond to $\beta < 0$ which are operationally similar to the KN case discussed in [184], and the solid curves correspond to $\beta > 0$. The solid black curve indicates the Kerr case ($\beta = 0$). In general, $\mathrm{Im}(\omega M)$ increases with the mass μM of the scalar field and becomes positive. It then reaches a maximum value[4] for some value of μM and on reaching this maximum, it decreases further with increasing μM and eventually becomes negative. In the mass range where $\mathrm{Im}(\omega) > 0, \mathrm{Re}(\omega) < \omega_c$. It is interesting to note from Fig. 8 that:

(i) for $a = 0.9M$ (left panel of Fig. 8), the presence of a relatively large positive tidal charge suppresses the superradiant instability by roughly two orders of magnitude. For $\beta = -0.99\beta_0$, (i.e., when the BH is near-extreme) we find the highest peak value of $\mathrm{Im}(\omega M) = 1.03832 \times 10^{-7}$ at $\mu M = 0.446114$ whereas for $\beta = 0.99\beta_0$, we observe the smallest peak value $\mathrm{Im}(\omega M) = 4.5619 \times 10^{-9}$ at $\mu M = 0.243645$. Note that for $\beta = 0$, we find a peak value of $\mathrm{Im}(\omega M) = 1.55244 \times 10^{-8}$ at $\mu M = 0.293274$.

(ii) for $a = 0.99M$ (middle panel of Fig. 8), we observe that the peak of the instability does not vary monotonically with β [184] and the peak occurs for a negative value of the tidal charge (corresponding to a subextreme configuration, in contrast to the previous case). The presence of a positive tidal charge is unable to significantly suppress the superradiant instability. For $\beta = -0.8\beta_0$, we find the highest peak value of $\mathrm{Im}(\omega M) = 1.64681 \times 10^{-7}$ at $\mu M = 0.452859$ whereas for $\beta = 0.99\beta_0$, we find the smallest peak value $\mathrm{Im}(\omega M) = 1.16555 \times 10^{-7}$ at $\mu M = 0.393733$. Note that for $\beta = 0$, we find a peak value of $\mathrm{Im}(\omega M) = 1.50435 \times 10^{-7}$ at $\mu M = 0.42082$. These results are consistent with [184].

(iii) for $a = 0.997M$ (right panel of Fig. 8), we obtain the maximum instability of $\mathrm{Im}(\omega M) = 1.72275 \times 10^{-7}$ for $\beta = 0$ at $\mu M = 0.450511$ which is again consistent with [184]. Interestingly enough, now the smallest positive value of β that we had considered has a higher peak than all the negative values of β. Note that for $\beta = 0.8\beta_0$, we find the peak value of $\mathrm{Im}(\omega M) = 1.70475 \times 10^{-7}$ at $\mu M = 0.439384$ whereas for $\beta = -0.99\beta_0$, we find the smallest peak value $\mathrm{Im}(\omega M) = 1.60246 \times 10^{-7}$ at $\mu M = 0.449493$.

(iv) If one were to solely focus on the positive values of the tidal charge, i.e., $\beta > 0$ but $a/M < 1$, it is clear from the three insets in Fig. 8, that decreasing β enhances the superradiant instability, and the corresponding peak values also increases with increase in a. But they always remain smaller than the corresponding peak values for $\beta = 0$. This appears to be consistent with the findings of [142] where the author studied the superradiant instability by examining the amplification factors of massless scalar fields scattered by a rotating braneworld BH.

Let us now talk about the case when $a/M = 1$. The results are visualized in Fig. 9. In this case, the value of $\beta_0 = 0$ corresponds to the extreme Kerr BH. So we take a few representative values of $\beta/M^2 > 0$ to study the superradiant instability and do not normalize the value of β.

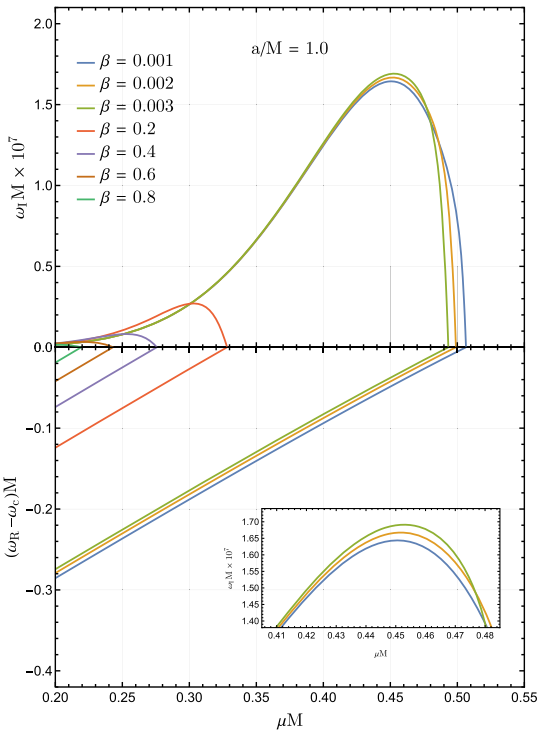

FIG. 9. The superradiant instability associated with the quasibound state spectrum of a massive neutral scalar field ($l = m = 1$) for $a/M = 1$ and different values of the tidal charge β (normalized with respect to M).

[4]We can find the maximum of the curve by constructing an interpolating function using the data generated by the continued fraction method. The function can then be maximized using standard techniques.

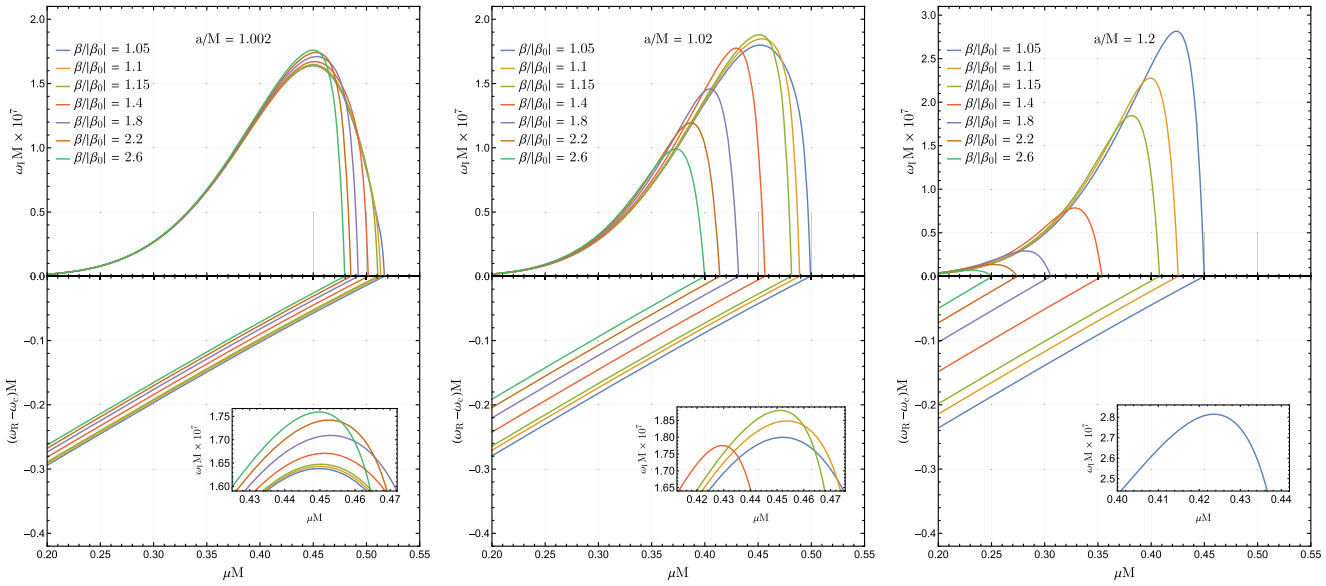

FIG. 10. The superradiant instability associated with the quasibound state spectrum of a massive neutral scalar field ($l = m = 1$) for different values of BH spin $a/M > 1$ and tidal charge β.

We do not study the $\beta = 0, a/M = 1$ case because our numerical method is not equipped to handle extreme BHs. To study extreme BHs, the modification of Leaver's original method suggested in [216,217] might be useful. We notice that moderate values tidal charge (that is, subextremal configurations) are able to significantly suppress the instability whereas the instability is enhanced in the presence of small positive values tidal charges. But intriguingly, the maximum instability *does not occur* for the smallest value of β considered. The maximum instability of $\mathrm{Im}(\omega M) = 1.6912 \times 10^{-7}$ occurs for $\beta = 0.003M^2$ at $\mu M = 0.45278$, and we get the smallest peak value of $\mathrm{Im}(\omega M) = 1.57103 \times 10^{-9}$ for $\beta = 0.8M^2$ at $\mu M = 0.202154$. Note that for $\beta = 0.001M^2$, the peak value is $\mathrm{Im}(\omega M) = 1.64362 \times 10^{-7}$ at $\mu M = 0.45062$.

We now come to the case when $a > 1$. In Fig. 10, we consider three values of $a = 1.002M, 1.02M, 1.2M$ and suitably normalized values of the tidal charge $\beta/M^2 > 0$ as earlier. We summarize our findings below:

(i) for $a = 1.002M$ (left panel of Fig. 10), the value of the peak of the instability increases with increasing the tidal charge. In particular, the maximum value of the peak $\mathrm{Im}(\omega M) = 1.7595 \times 10^{-7}$ occurs for $\beta = 2.6\beta_0$ at $\mu M = 0.449823$. Note that for the instability is the least for $\beta = 1.05\beta_0$ with a peak value of $\mathrm{Im}(\omega M) = 1.63817 \times 10^{-7}$ at $\mu M = 0.449787$.

(ii) for $a = 1.02M$ (middle panel of Fig. 10), we again see that the peak of the instability does not vary monotonically with β. The maximum peak occurs for and intermediate value of $\beta = 1.15\beta_0$ at $\mathrm{Im}(\omega M) = 1.87952 \times 10^{-7}$ for $\mu M = 0.451168$.

(iii) for $a = 1.2M$ (right panel of Fig. 10), we notice a behavior opposite to the one encounter for $a = 1.002$. We now see that increasing the tidal charge suppresses the superradiant instability by roughly a couple of orders of magnitude. For $\beta = 1.05\beta_0$, we find the highest peak value of $\mathrm{Im}(\omega M) = 2.8151 \times 10^{-7}$ at $\mu M = 0.423676$ whereas for $\beta = 2.6\beta_0$, we observe the smallest peak value $\mathrm{Im}(\omega M) = 7.17095 \times 10^{-9}$ at $\mu M = 0.230162$.

(iv) if we focus on $\beta = 1.05\beta_0$ which by design corresponds to a near-extreme BH for all the three values of a that we have considered, we see from the insets in Fig. 10 that the superradiant instability for near extreme BHs with $a/M > 1$ intensifies with increase in the value of a (and also the bare value of the tidal charge β). Looking at the same for $\beta = 2.6\beta_0$, the opposite conclusion holds for subextremal braneworld black holes.

Lastly, in Fig. 11 we keep the tidal charge fixed at $\beta = 0.5M^2$, and study the superradiant instability by varying a whose values are normalized with respect to $a_{\mathrm{max}}/M = \sqrt{1 + \beta/M^2}$. We note that the superradiant instability intensifies as a increases. In particular, the maximum value of the peak is $\mathrm{Im}(\omega M) = 3.12115 \times 10^{-7}$ at $\mu M = 0.438173$ for a near-extreme BH with $a = 1.21974M^2$, or $a = 0.995918a_{\mathrm{max}}$.

We summarize our results for the maximum peak of the superradiant instability for various values of a and β in Table I.

We end this section with a few comments: First, we note that all of our figures clearly show that instability $\mathrm{Im}(\omega) > 0$ always occurs in the superradiant regime, $0 < \mathrm{Re}(\omega) < \omega_c$. Second, it is in general very difficult to accurately determine for what values of a, β, μ, the superradiant instability will be maximum. However, based

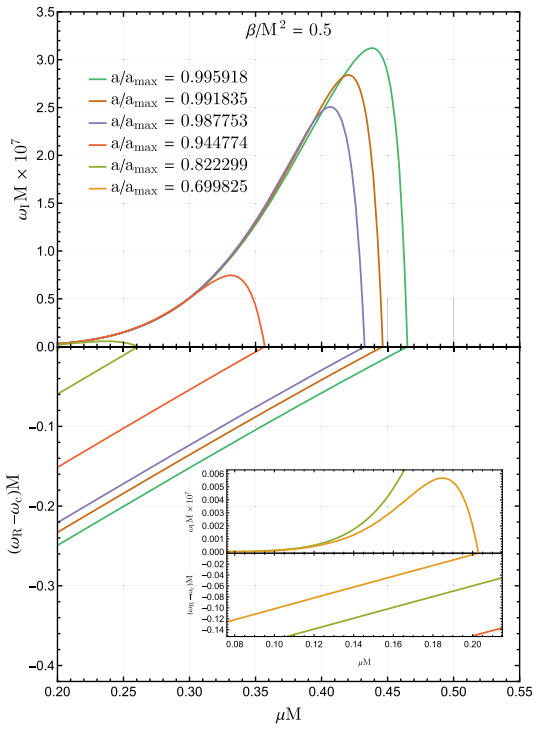

FIG. 11. The superradiant instability associated with the quasibound state spectrum of a neutral scalar field ($l = m = 1$) for different values of BH spin $a/M > 1$ and fixed tidal charge β.

on our numerical study we may conclude that (i) for $\beta > 0$ and $a/M < 1$, a higher value of the tidal charge would dampen the instability, (ii) for $\beta > 0$ and $a/M \geq 1$, the maximum superradiant instability does not vary monotonically with β but the order of the maximum value is the same as that of the Kerr black hole. The behavior is highly nontrivial, especially when one compares it to results reported previously for massless scalar fields [142].

VI. FINAL REMARKS

The RS II rotating braneworld black hole solution provides us with a springboard to test the presence of an extra noncompact spatial dimension on gravitational interactions in the strong field regime. In this study, we have focused on the behavior of a massive scalar field with $\mu M < 1$ propagating in the said black hole spacetime. Since the braneworld BH can be superspinning, we have focused on the region of the parameter space where $a/M > 1$ and $\beta > 0$. First, we have made an in-depth study of the quasinormal mode spectra of massive scalar perturbations and have noted the intricate behavior shown by the modes corresponding to different values of the azimuthal number m for $l = 1$. The behavior is qualitatively similar to that of the Kerr (Newman) black hole [191–193]. We have further explored the formation of quasiresonance modes and discussed the existence of zero damped modes as well.

Next, we have studied the $l = m = 1$ quasibound states and superradiant instability associated with such modes, that is, the formation of the so-called gravitational atom. Our analysis reveals a highly nontrivial dependence of the peak of the superradiant instability on the tidal charge and the angular momentum of the black hole. For $a/M < 1$, the presence of the tidal charge always dampens the superradiant instability when one compares it to that of the Kerr BH. However, the dynamics is much richer when one looks at superspinning ($a/M > 1$) configurations. Notably, for such near extremal BHs, the superradiant instability intensifies with the tidal charge, although the maximum superradiant instability is comparable to that of the Kerr black hole. These findings could have implications for ongoing efforts to detect boson clouds around black holes in order to constrain the mass of ultra light particles [172,173,177].

The present work offers numerous extensions. We are attempting to investigate the phenomena of eigenvalue repulsion [218,219] in the quasinormal mode spectra of the rotating braneworld black hole. Moreover, it has been pointed out that the QNM spectrum of black holes may be unstable against small perturbations to the scattering potential [202,220]. It would be worthwhile to study the effect of the tidal charge on the instability of the QNM spectrum. One can also construct braneworld BH solutions which are not asymptotically flat [221] and one may use these solutions to understand how the presence of both the cosmological constant and the extra dimension change the behavior of the QNM spectrum. It would also be interesting to see how the presence of the tidal charge affects the superradiant instability in the regime $\mu \sim \omega$ when the scalar field is charged following [184,198]. Lastly, both scalar and vector boson clouds around Kerr BHs have attracted a lot of attention in recent years, especially in the context of gravitational wave astronomy with binary black holes and people have already explored various aspects of such gravitational atoms [173–176,222–229]. It would be interesting to extend these studies to the braneworld scenario. Note that in [230], the superradiant instability and the formation of the vector gravitational atom was studied for the Kerr Newman black hole. Such a pioneering investigation was possible only after solving the difficult problem of separating the Proca equation by exploiting certain hidden symmetries of the spacetime. Our preliminary investigations indicate that many of these problems

TABLE I. Maximum peaks of superradiant instability.

a/M	β/M^2	μM	$\mathrm{Im}(\omega M)$
0.9	−0.1881000	0.446114	1.03832×10^{-7}
0.99	−0.0159200	0.452859	1.64681×10^{-7}
0.997	0	0.450511	1.72275×10^{-7}
1.0	0.003	0.45278	1.6912×10^{-7}
1.002	0.0104104	0.449823	1.7595×10^{-7}
1.02	0.0464600	0.451168	1.87952×10^{-7}
1.2	0.4620000	0.423676	2.8151×10^{-7}
1.21974	0.5	0.438173	3.12115×10^{-7}

can be extended in to the braneworld scenario and the presence of the tidal charge will leave a clear mark of the extra dimension on these systems. We wish to study some of these aspects in the future.

ACKNOWLEDGMENTS

The authors would like to thank Mostafizur Rahman, Srijit Bhattacharjee and Sumanta Chakraborty for useful discussions. S. S. acknowledges funding from SERB, DST, Government of India through the Core Research Grant No. CRG/2020/004347. A. A. S. acknowledges the funding from SERB, Govt. of India under the Core Research Grant No. CRG/2020/004347. S. S. B. acknowledges the funding from the University Grants Commission, Govt. of India under JRF scheme.

[1] B. P. Abbott *et al.* (LIGO Scientific and Virgo Collaborations), Observation of gravitational waves from a binary black hole merger, Phys. Rev. Lett. **116**, 061102 (2016).
[2] B. P. Abbott *et al.* (LIGO Scientific and Virgo Collaborations), GW170817: Observation of gravitational waves from a binary neutron star inspiral, Phys. Rev. Lett. **119**, 161101 (2017).
[3] B. P. Abbott *et al.* (LIGO Scientific and Virgo Collaborations), GWTC-1: A gravitational-wave transient catalog of compact binary mergers observed by LIGO and Virgo during the first and second observing runs, Phys. Rev. X **9**, 031040 (2019).
[4] K. Akiyama *et al.* (Event Horizon Telescope Collaboration), First M87 event horizon telescope results. I. The shadow of the supermassive black hole, Astrophys. J. Lett. **875**, L1 (2019).
[5] K. Akiyama *et al.* (Event Horizon Telescope Collaboration), First M87 event horizon telescope results. IV. Imaging the central supermassive black hole, Astrophys. J. Lett. **875**, L4 (2019).
[6] K. Akiyama *et al.* (Event Horizon Telescope Collaboration), First M87 event horizon telescope results. VII. Polarization of the ring, Astrophys. J. Lett. **910**, L12 (2021).
[7] K. Akiyama *et al.* (Event Horizon Telescope Collaboration), First M87 event horizon telescope results. VIII. Magnetic field structure near the event horizon, Astrophys. J. Lett. **910**, L13 (2021).
[8] K. Akiyama *et al.* (Event Horizon Telescope Collaboration), First M87 event horizon telescope results. IX. Detection of near-horizon circular polarization, Astrophys. J. Lett. **957**, L20 (2023).
[9] K. Akiyama *et al.* (Event Horizon Telescope Collaboration), First Sagittarius A* event horizon telescope results. I. The shadow of the supermassive black hole in the center of the Milky Way, Astrophys. J. Lett. **930**, L12 (2022).
[10] K. Akiyama *et al.* (Event Horizon Telescope Collaboration), First Sagittarius A* event horizon telescope results. III. Imaging of the Galactic Center supermassive black hole, Astrophys. J. Lett. **930**, L14 (2022).
[11] R. Abuter *et al.* (GRAVITY Collaboration), Detection of the gravitational redshift in the orbit of the star S2 near the Galactic centre massive black hole, Astron. Astrophys. **615**, L15 (2018).
[12] T. Do *et al.*, Relativistic redshift of the star S0-2 orbiting the Galactic Center supermassive black hole, Science **365**, 664 (2019).
[13] R. Abuter *et al.* (GRAVITY Collaboration), Detection of the Schwarzschild precession in the orbit of the star S2 near the Galactic centre massive black hole, Astron. Astrophys. **636**, L5 (2020).
[14] O. Dreyer, B. J. Kelly, B. Krishnan, L. S. Finn, D. Garrison, and R. Lopez-Aleman, Black hole spectroscopy: Testing general relativity through gravitational wave observations, Classical Quantum Gravity **21**, 787 (2004).
[15] E. Berti, K. Yagi, and N. Yunes, Extreme gravity tests with gravitational waves from compact binary coalescences: (I) Inspiral-merger, Gen. Relativ. Gravit. **50**, 46 (2018).
[16] E. Berti, K. Yagi, H. Yang, and N. Yunes, Extreme gravity tests with gravitational waves from compact binary coalescences: (II) Ringdown, Gen. Relativ. Gravit. **50**, 49 (2018).
[17] K. Yagi and L. C. Stein, Black hole based tests of general relativity, Classical Quantum Gravity **33**, 054001 (2016).
[18] K. Hioki and K.-i. Maeda, Measurement of the Kerr spin parameter by observation of a compact object's shadow, Phys. Rev. D **80**, 024042 (2009).
[19] C. Bambi, Can the supermassive objects at the centers of galaxies be traversable wormholes? The first test of strong gravity for mm/sub-mm very long baseline interferometry facilities, Phys. Rev. D **87**, 107501 (2013).
[20] C. Bambi, Testing black hole candidates with electromagnetic radiation, Rev. Mod. Phys. **89**, 025001 (2017).
[21] P. V. P. Cunha and C. A. R. Herdeiro, Shadows and strong gravitational lensing: A brief review, Gen. Relativ. Gravit. **50**, 42 (2018).
[22] R. Narayan, M. D. Johnson, and C. F. Gammie, The shadow of a spherically accreting black hole, Astrophys. J. Lett. **885**, L33 (2019).
[23] S. E. Gralla, D. E. Holz, and R. M. Wald, Black hole shadows, photon rings, and lensing rings, Phys. Rev. D **100**, 024018 (2019).
[24] D. Psaltis *et al.* (Event Horizon Telescope Collaboration), Gravitational test beyond the first post-Newtonian order with the shadow of the M87 black hole, Phys. Rev. Lett. **125**, 141104 (2020).
[25] C. Bambi, K. Freese, S. Vagnozzi, and L. Visinelli, Testing the rotational nature of the supermassive object M87* from

the circularity and size of its first image, Phys. Rev. D **100**, 044057 (2019).
[26] A. Amorim *et al.* (GRAVITY Collaboration), Test of the Einstein equivalence principle near the Galactic Center supermassive black hole, Phys. Rev. Lett. **122**, 101102 (2019).
[27] C. M. Will, Was Einstein right?: Testing relativity at the centenary, Ann. Phys. (Berlin) **15**, 19 (2005).
[28] C. M. Will, Resource letter PTG-1: Precision tests of gravity, Am. J. Phys. **78**, 1240 (2010).
[29] C. M. Will, The confrontation between general relativity and experiment, Living Rev. Relativity **17**, 4 (2014).
[30] C. M. Will, *Theory and Experiment in Gravitational Physics* (Cambridge University Press, Cambridge, England, 2018).
[31] B. P. Abbott *et al.* (LIGO Scientific and Virgo Collaborations), Properties of the binary black hole merger GW150914, Phys. Rev. Lett. **116**, 241102 (2016).
[32] B. P. Abbott *et al.* (LIGO Scientific and Virgo Collaborations), Tests of general relativity with GW150914, Phys. Rev. Lett. **116**, 221101 (2016); **121**, 129902(E) (2018).
[33] B. P. Abbott *et al.* (LIGO Scientific and Virgo Collaborations), GW170104: Observation of a 50-solar-mass binary black hole coalescence at redshift 0.2, Phys. Rev. Lett. **118**, 221101 (2017); **121**, 129901(E) (2018).
[34] B. P. Abbott *et al.* (LIGO Scientific and Virgo Collaborations), Tests of general relativity with GW170817, Phys. Rev. Lett. **123**, 011102 (2019).
[35] B. P. Abbott *et al.* (LIGO Scientific and Virgo Collaborations), Tests of general relativity with the binary black hole signals from the LIGO-Virgo catalog GWTC-1, Phys. Rev. D **100**, 104036 (2019).
[36] R. Abbott *et al.* (LIGO Scientific and Virgo Collaborations), Tests of general relativity with binary black holes from the second LIGO-Virgo gravitational-wave transient catalog, Phys. Rev. D **103**, 122002 (2021).
[37] R. Abbott *et al.* (LIGO Scientific, VIRGO, and KAGRA Collaborations), Tests of general relativity with GWTC-3, arXiv:2112.06861.
[38] K. Akiyama *et al.* (Event Horizon Telescope Collaboration), First M87 event horizon telescope results. VI. The shadow and mass of the central black hole, Astrophys. J. Lett. **875**, L6 (2019).
[39] P. Kocherlakota *et al.* (Event Horizon Telescope Collaboration), Constraints on black-hole charges with the 2017 EHT observations of M87*, Phys. Rev. D **103**, 104047 (2021).
[40] K. Akiyama *et al.* (Event Horizon Telescope Collaboration), First Sagittarius A* event horizon telescope results. VI. Testing the black hole metric, Astrophys. J. Lett. **930**, L17 (2022).
[41] E. Berti, A. Buonanno, and C. M. Will, Estimating spinning binary parameters and testing alternative theories of gravity with LISA, Phys. Rev. D **71**, 084025 (2005).
[42] V. Cardoso, L. Gualtieri, C. Herdeiro, and U. Sperhake, Exploring new physics frontiers through numerical relativity, Living Rev. Relativity **18**, 1 (2015).
[43] E. Berti *et al.*, Testing general relativity with present and future astrophysical observations, Classical Quantum Gravity **32**, 243001 (2015).
[44] L. Barack *et al.*, Black holes, gravitational waves and fundamental physics: A roadmap, Classical Quantum Gravity **36**, 143001 (2019).
[45] N. Yunes and X. Siemens, Gravitational-wave tests of general relativity with ground-based detectors and pulsar timing-arrays, Living Rev. Relativity **16**, 9 (2013).
[46] E. Cannizzaro, G. Franciolini, and P. Pani, Novel tests of gravity using nano-Hertz stochastic gravitational-wave background signals, arXiv:2307.11665.
[47] P. Amaro-Seoane *et al.*, Low-frequency gravitational-wave science with eLISA/NGO, Classical Quantum Gravity **29**, 124016 (2012).
[48] E. Berti *et al.*, Tests of general relativity and fundamental physics with space-based gravitational wave detectors, arXiv:1903.02781.
[49] E. Barausse *et al.*, Prospects for fundamental physics with LISA, Gen. Relativ. Gravit. **52**, 81 (2020).
[50] K. G. Arun *et al.* (LISA Collaboration), New horizons for fundamental physics with LISA, Living Rev. Relativity **25**, 4 (2022).
[51] J. Luo *et al.* (TianQin Collaboration), TianQin: A space-borne gravitational wave detector, Classical Quantum Gravity **33**, 035010 (2016).
[52] M. A. Abramowicz, W. Kluzniak, and J.-P. Lasota, No observational prot the black hole event-horizon, Astron. Astrophys. **396**, L31 (2002).
[53] V. Cardoso, E. Franzin, and P. Pani, Is the gravitational-wave ringdown a probe of the event horizon?, Phys. Rev. Lett. **116**, 171101 (2016); **117**, 089902(E) (2016).
[54] V. Cardoso and P. Pani, Testing the nature of dark compact objects: A status report, Living Rev. Relativity **22**, 4 (2019).
[55] Y. Mizuno, Z. Younsi, C. M. Fromm, O. Porth, M. De Laurentis, H. Olivares, H. Falcke, M. Kramer, and L. Rezzolla, The current ability to test theories of gravity with black hole shadows, Nat. Astron. **2**, 585 (2018).
[56] S. E. Gralla, Can the EHT M87 results be used to test general relativity?, Phys. Rev. D **103**, 024023 (2021).
[57] R. Penrose, Gravitational collapse and space-time singularities, Phys. Rev. Lett. **14**, 57 (1965).
[58] S. W. Hawking, Breakdown of predictability in gravitational collapse, Phys. Rev. D **14**, 2460 (1976).
[59] D. Christodoulou, The formation of black holes and singularities in spherically symmetric gravitational collapse, Commun. Pure Appl. Math. **44**, 339 (1991).
[60] A. Ori, Inner structure of a charged black hole: An exact mass-inflation solution, Phys. Rev. Lett. **67**, 789 (1991).
[61] M. Dafermos, The interior of charged black holes and the problem of uniqueness in general relativity, Commun. Pure Appl. Math. **58**, 0445 (2005).
[62] S. Bhattacharjee, S. Sarkar, and A. Virmani, Internal structure of charged AdS black holes, Phys. Rev. D **93**, 124029 (2016).
[63] V. Cardoso, J. a. L. Costa, K. Destounis, P. Hintz, and A. Jansen, Quasinormal modes and strong cosmic censorship, Phys. Rev. Lett. **120**, 031103 (2018).
[64] O. J. C. Dias, H. S. Reall, and J. E. Santos, The BTZ black hole violates strong cosmic censorship, J. High Energy Phys. 12 (2019) 097.

[65] M. Rahman, On the validity of Strong cosmic censorship conjecture in presence of Dirac fields, Eur. Phys. J. C **80**, 360 (2020).
[66] M. Rahman, S. Mitra, and S. Chakraborty, Strong cosmic censorship conjecture with NUT charge and conformal coupling, Classical Quantum Gravity **37**, 195004 (2020).
[67] M. Rahman, Gravity in modified theories, Ph.D. thesis, Jamia Milia Islamia University, Centre for Theoretical Physics, India, 2020.
[68] S. Bhattacharjee, S. Kumar, and S. Sarkar, Mass inflation and strong cosmic censorship in a nonextreme BTZ black hole, Phys. Rev. D **102**, 044030 (2020).
[69] S. Bhattacharjee, S. Sarkar, and A. Bhattacharyya, Scalar perturbations of black holes in Jackiw-Teitelboim gravity, Phys. Rev. D **103**, 024008 (2021).
[70] S. W. Hawking, Particle creation by black holes, Commun. Math. Phys. **43**, 199 (1975); **46**, 206(E) (1976).
[71] S. Chakraborty and K. Lochan, Black holes: Eliminating information or illuminating new physics?, Universe **3**, 55 (2017).
[72] S. D. Mathur, The information paradox: A pedagogical introduction, Classical Quantum Gravity **26**, 224001 (2009).
[73] S. Perlmutter *et al.* (Supernova Cosmology Project Collaboration), Measurements of Ω and Λ from 42 high redshift supernovae, Astrophys. J. **517**, 565 (1999).
[74] A. G. Riess *et al.* (Supernova Search Team), Observational evidence from supernovae for an accelerating universe and a cosmological constant, Astron. J. **116**, 1009 (1998).
[75] V. Sahni and A. A. Starobinsky, The case for a positive cosmological Lambda term, Int. J. Mod. Phys. D **09**, 373 (2000).
[76] T. Padmanabhan, Cosmological constant: The weight of the vacuum, Phys. Rep. **380**, 235 (2003).
[77] P. J. E. Peebles and B. Ratra, The cosmological constant and dark energy, Rev. Mod. Phys. **75**, 559 (2003).
[78] V. C. Rubin, W. K. Ford, Jr., and N. Thonnard, Extended rotation curves of high-luminosity spiral galaxies. IV. Systematic dynamical properties, Sa through Sc, Astrophys. J. Lett. **225**, L107 (1978).
[79] G. Bertone and D. Hooper, History of dark matter, Rev. Mod. Phys. **90**, 045002 (2018).
[80] S. Nojiri and S. D. Odintsov, Introduction to modified gravity and gravitational alternative for dark energy, Int. J. Geom. Methods Mod. Phys. **04**, 115 (2007).
[81] T. Clifton, P. G. Ferreira, A. Padilla, and C. Skordis, Modified gravity and cosmology, Phys. Rep. **513**, 1 (2012).
[82] S. Nojiri, S. D. Odintsov, and V. K. Oikonomou, Modified gravity theories on a nutshell: Inflation, bounce and late-time evolution, Phys. Rep. **692**, 1 (2017).
[83] S. Shankaranarayanan and J. P. Johnson, Modified theories of gravity: Why, how and what?, Gen. Relativ. Gravit. **54**, 44 (2022).
[84] S. D. Odintsov, V. K. Oikonomou, I. Giannakoudi, F. P. Fronimos, and E. C. Lymperiadou, Recent advances in inflation, Symmetry **15**, 1701 (2023).
[85] S. Nojiri and S. D. Odintsov, Unified cosmic history in modified gravity: From F(R) theory to Lorentz non-invariant models, Phys. Rep. **505**, 59 (2011).
[86] A. De Felice and S. Tsujikawa, f(R) theories, Living Rev. Relativity **13**, 3 (2010).
[87] T. Padmanabhan and D. Kothawala, Lanczos-Lovelock models of gravity, Phys. Rep. **531**, 115 (2013).
[88] S. F. Hassan and R. A. Rosen, Bimetric gravity from ghost-free massive gravity, J. High Energy Phys. 02 (2012) 126.
[89] E. Babichev and M. Crisostomi, Restoring general relativity in massive bigravity theory, Phys. Rev. D **88**, 084002 (2013).
[90] M. Rahman, A. A. Sen, and S. S. Bohra, Traversable wormholes in bimetric gravity, Phys. Rev. D **108**, 104008 (2023).
[91] G. W. Horndeski, Second-order scalar-tensor field equations in a four-dimensional space, Int. J. Theor. Phys. **10**, 363 (1974).
[92] T. P. Sotiriou and S.-Y. Zhou, Black hole hair in generalized scalar-tensor gravity, Phys. Rev. Lett. **112**, 251102 (2014).
[93] E. Babichev, C. Charmousis, and A. Lehébel, Black holes and stars in Horndeski theory, Classical Quantum Gravity **33**, 154002 (2016).
[94] L. Heisenberg, Generalization of the proca action, J. Cosmol. Astropart. Phys. 05 (2014) 015.
[95] A. De Felice, L. Heisenberg, R. Kase, S. Tsujikawa, Y.-l. Zhang, and G.-B. Zhao, Screening fifth forces in generalized Proca theories, Phys. Rev. D **93**, 104016 (2016).
[96] M. Rahman and A. A. Sen, Astrophysical signatures of black holes in generalized Proca theories, Phys. Rev. D **99**, 024052 (2019).
[97] J. M. Overduin and P. S. Wesson, Kaluza-Klein gravity, Phys. Rep. **283**, 303 (1997).
[98] S. Raychaudhuri and K. Sridhar, *Particle Physics of Brane Worlds and Extra Dimensions*, Cambridge Monographs on Mathematical Physics (Cambridge University Press, Cambridge, England, 2016), 10.1017/CBO9781139045650.
[99] L. Randall and R. Sundrum, A large mass hierarchy from a small extra dimension, Phys. Rev. Lett. **83**, 3370 (1999).
[100] L. Randall and R. Sundrum, An alternative to compactification, Phys. Rev. Lett. **83**, 4690 (1999).
[101] A. Chamblin, S. W. Hawking, and H. S. Reall, Brane world black holes, Phys. Rev. D **61**, 065007 (2000).
[102] A. Chamblin, H. S. Reall, H.-a. Shinkai, and T. Shiromizu, Charged brane world black holes, Phys. Rev. D **63**, 064015 (2001).
[103] T. Shiromizu, K.-i. Maeda, and M. Sasaki, The Einstein equation on the 3-brane world, Phys. Rev. D **62**, 024012 (2000).
[104] M. Sasaki, T. Shiromizu, and K.-i. Maeda, Gravity, stability and energy conservation on the Randall-Sundrum brane world, Phys. Rev. D **62**, 024008 (2000).
[105] T. Harko and M. K. Mak, Vacuum solutions of the gravitational field equations in the brane world model, Phys. Rev. D **69**, 064020 (2004).
[106] A. N. Aliev and A. E. Gumrukcuoglu, Gravitational field equations on and off a 3-brane world, Classical Quantum Gravity **21**, 5081 (2004).
[107] J. Garriga and T. Tanaka, Gravity in the brane world, Phys. Rev. Lett. **84**, 2778 (2000).
[108] S. B. Giddings, E. Katz, and L. Randall, Linearized gravity in brane backgrounds, J. High Energy Phys. 03 (2000) 023.

[109] R. Maartens, Cosmological dynamics on the brane, Phys. Rev. D **62**, 084023 (2000).
[110] R. Maartens, Geometry and dynamics of the brane world, in *Proceedings of the Spanish Relativity Meeting on Reference Frames and Gravitomagnetism (EREs2000)* (2001) arXiv:gr-qc/0101059.
[111] N. Dadhich, R. Maartens, P. Papadopoulos, and V. Rezania, Black holes on the brane, Phys. Lett. B **487**, 1 (2000).
[112] A. N. Aliev and A. E. Gumrukcuoglu, Charged rotating black holes on a 3-brane, Phys. Rev. D **71**, 104027 (2005).
[113] A. N. Aliev, Rotating braneworld black holes, in *Proceedings of the 11th Marcel Grossmann Meeting on General Relativity* (2006), pp. 2830–2832 arXiv:astro-ph/0612735.
[114] A. N. Aliev and P. Talazan, Gravitational effects of rotating braneworld black holes, Phys. Rev. D **80**, 044023 (2009).
[115] A. N. Aliev, G. D. Esmer, and P. Talazan, Strong gravity effects of rotating black holes: Quasiperiodic oscillations, Classical Quantum Gravity **30**, 045010 (2013).
[116] S. Bhattacharya, D. Choudhury, D. P. Jatkar, and A. A. Sen, Brane dynamics in the Randall-Sundrum model, inflation and graceful exit, Classical Quantum Gravity **19**, 5025 (2002).
[117] M. C. Bento, O. Bertolami, and A. A. Sen, Supergravity inflation on the brane, Phys. Rev. D **67**, 023504 (2003).
[118] M. C. Bento, O. Bertolami, and A. A. Sen, Tachyonic inflation in the brane world scenario, Phys. Rev. D **67**, 063511 (2003).
[119] B. Mukhopadhyaya, S. Sen, and S. SenGupta, Does a Randall-Sundrum scenario create the illusion of a torsion free universe?, Phys. Rev. Lett. **89**, 121101 (2002); **89**, 259902(E) (2002).
[120] Y.-b. Kim, C. O. Lee, I.-b. Lee, and J.-J. Lee, Brane world of warp geometry: An introductory review, J. Korean Astron. Soc. **37**, 1 (2004).
[121] P. Kanti, Black holes in theories with large extra dimensions: A review, Int. J. Mod. Phys. A **19**, 4899 (2004).
[122] A. Perez-Lorenzana, An introduction to extra dimensions, J. Phys. Conf. Ser. **18**, 224 (2005).
[123] R. Maartens and K. Koyama, Brane-world gravity, Living Rev. Relativity **13**, 5 (2010).
[124] T. Nakas and P. Kanti, Localized brane-world black hole analytically connected to an AdS_5 boundary, Phys. Lett. B **816**, 136278 (2021).
[125] T. Nakas and P. Kanti, Analytic and exponentially localized braneworld Reissner-Nordström-AdS solution: A top-down approach, Phys. Rev. D **104**, 104037 (2021).
[126] T. Nakas, T. D. Pappas, and Z. Stuchlík, Bridging dimensions: General embedding algorithm and field-theory reconstruction in 5D braneworld models, Phys. Rev. D **109**, L041501 (2024).
[127] T. Adamo and E. T. Newman, The Kerr-Newman metric: A review, Scholarpedia **9**, 31791 (2014).
[128] D. J. H. Chung, L. L. Everett, and H. Davoudiasl, Experimental probes of the Randall-Sundrum infinite extra dimension, Phys. Rev. D **64**, 065002 (2001).
[129] A. Y. Bin-Nun, Relativistic images in Randall-Sundrum II braneworld lensing, Phys. Rev. D **81**, 123011 (2010).
[130] A. Y. Bin-Nun, Lensing By Sgr A^* as a probe of modified gravity, Phys. Rev. D **82**, 064009 (2010).
[131] L. Amarilla and E. F. Eiroa, Shadow of a rotating braneworld black hole, Phys. Rev. D **85**, 064019 (2012).
[132] I. Banerjee, S. Chakraborty, and S. SenGupta, Silhouette of M87*: A new window to peek into the world of hidden dimensions, Phys. Rev. D **101**, 041301 (2020).
[133] I. Banerjee, S. Chakraborty, and S. SenGupta, Decoding signatures of extra dimensions and estimating spin of quasars from the continuum spectrum, Phys. Rev. D **100**, 044045 (2019).
[134] S. Vagnozzi and L. Visinelli, Hunting for extra dimensions in the shadow of M87*, Phys. Rev. D **100**, 024020 (2019).
[135] J. C. S. Neves, Constraining the tidal charge of brane black holes using their shadows, Eur. Phys. J. C **80**, 717 (2020).
[136] I. Banerjee, S. Chakraborty, and S. SenGupta, Hunting extra dimensions in the shadow of Sgr A^*, Phys. Rev. D **106**, 084051 (2022).
[137] J.-y. Shen, B. Wang, and R.-K. Su, The signals from the brane-world black hole, Phys. Rev. D **74**, 044036 (2006).
[138] B. Toshmatov, Z. Stuchlík, J. Schee, and B. Ahmedov, Quasinormal frequencies of black hole in the braneworld, Phys. Rev. D **93**, 124017 (2016).
[139] A. Chowdhury and N. Banerjee, Quasinormal modes of a charged spherical black hole with scalar hair for scalar and Dirac perturbations, Eur. Phys. J. C **78**, 594 (2018).
[140] A. K. Mishra, A. Ghosh, and S. Chakraborty, Constraining extra dimensions using observations of black hole quasinormal modes, Eur. Phys. J. C **82**, 820 (2022).
[141] A. K. Mishra, G. Carullo, and S. Chakraborty, Bounds on tidal charges from gravitational-wave ringdown observations, Phys. Rev. D **109**, 024025 (2024).
[142] E. S. de Oliveira, Tidal-charge effects on the superradiance of rotating black holes, Eur. Phys. J. C **80**, 1048 (2020).
[143] S. Biswas, Massive scalar perturbation of extremal rotating braneworld black hole: Superradiant stability analysis, Phys. Lett. B **820**, 136597 (2021).
[144] S. Chakraborty, K. Chakravarti, S. Bose, and S. SenGupta, Signatures of extra dimensions in gravitational waves from black hole quasinormal modes, Phys. Rev. D **97**, 104053 (2018).
[145] L. Visinelli, N. Bolis, and S. Vagnozzi, Brane-world extra dimensions in light of GW170817, Phys. Rev. D **97**, 064039 (2018).
[146] M. Rahman, S. Chakraborty, S. SenGupta, and A. A. Sen, Fate of strong cosmic censorship conjecture in presence of higher spacetime dimensions, J. High Energy Phys. 03 (2019) 178.
[147] R. Dey, S. Chakraborty, and N. Afshordi, Echoes from braneworld black holes, Phys. Rev. D **101**, 104014 (2020).
[148] R. Dey, S. Biswas, and S. Chakraborty, Ergoregion instability and echoes for braneworld black holes: Scalar, electromagnetic, and gravitational perturbations, Phys. Rev. D **103**, 084019 (2021).
[149] S. Chakraborty, E. Maggio, A. Mazumdar, and P. Pani, Implications of the quantum nature of the black hole horizon on the gravitational-wave ringdown, Phys. Rev. D **106**, 024041 (2022).
[150] K. Chakravarti, S. Chakraborty, S. Bose, and S. SenGupta, Tidal Love numbers of black holes and neutron stars in the presence of higher dimensions: Implications of GW170817, Phys. Rev. D **99**, 024036 (2019).

[151] M. Rahman, S. Kumar, and A. Bhattacharyya, Gravitational wave from extreme mass-ratio inspirals as a probe of extra dimensions, J. Cosmol. Astropart. Phys. 01 (2023) 046.
[152] S. Mukherjee and S. Chakraborty, Transition from inspiral to plunge for braneworld EMRI, Classical Quantum Gravity **40**, 145013 (2023).
[153] A. Ghosh, R. Brito, and A. Buonanno, Constraints on quasinormal-mode frequencies with LIGO-Virgo binary–black-hole observations, Phys. Rev. D **103**, 124041 (2021).
[154] A. K. Mishra and S. Chakraborty, Strong cosmic censorship conjecture in higher curvature gravity, Phys. Rev. D **101**, 064041 (2020).
[155] A. Kotrlova, Z. Stuchlik, and G. Torok, Quasiperiodic oscillations in a strong gravitational field around neutron stars testing braneworld models, Classical Quantum Gravity **25**, 225016 (2008).
[156] A. Abdujabbarov and B. Ahmedov, Charged particle motion around rotating black hole in braneworld immersed in magnetic field, Phys. Rev. D **81**, 044022 (2010).
[157] A. F. Zakharov, Constraints on tidal charge of the supermassive black hole at the Galactic Center with trajectories of bright stars, Eur. Phys. J. C **78**, 689 (2018).
[158] H.-X. Zhang, C. Li, P.-Z. He, Q.-Q. Fan, and J.-B. Deng, Optical properties of a brane-world black hole as photons couple to the Weyl tensor, Eur. Phys. J. C **80**, 461 (2020).
[159] I. Banerjee, S. Chakraborty, and S. SenGupta, Looking for extra dimensions in the observed quasi-periodic oscillations of black holes, J. Cosmol. Astropart. Phys. 09 (2021) 037.
[160] E. S. de Oliveira, Scalar scattering from charged black holes on the brane, Classical Quantum Gravity **35**, 065007 (2018).
[161] E. S. de Oliveira, Scalar scattering from black holes with tidal charge, Eur. Phys. J. C **78**, 876 (2018).
[162] E. S. de Oliveira, Electromagnetic absorption, emission and scattering spectra of black holes with tidal charge, Eur. Phys. J. Plus **135**, 880 (2020).
[163] E. S. de Oliveira, Scalar absorption cross section of rotating black holes with tidal charge, Phys. Rev. D **104**, 124008 (2021).
[164] S. Biswas, M. Rahman, and S. Chakraborty, Echoes from braneworld wormholes, Phys. Rev. D **106**, 124003 (2022).
[165] C. V. Vishveshwara, Scattering of gravitational radiation by a Schwarzschild black-hole, Nature (London) **227**, 936 (1970).
[166] E. Berti, V. Cardoso, and A. O. Starinets, Quasinormal modes of black holes and black branes, Classical Quantum Gravity **26**, 163001 (2009).
[167] R. Konoplya and A. Zhidenko, Quasinormal modes of black holes: From astrophysics to string theory, Rev. Mod. Phys. **83**, 793 (2011).
[168] R. Brito, V. Cardoso, and P. Pani, Superradiance: New frontiers in black hole physics, Lect. Notes Phys. **906**, 1 (2015).
[169] W. H. Press and S. A. Teukolsky, Floating orbits, superradiant scattering and the black-hole bomb, Nature (London) **238**, 211 (1972).
[170] V. Cardoso, O. J. C. Dias, J. P. S. Lemos, and S. Yoshida, The black hole bomb and superradiant instabilities, Phys. Rev. D **70**, 044039 (2004); **70**, 049903(E) (2004).
[171] A. Arvanitaki, S. Dimopoulos, S. Dubovsky, N. Kaloper, and J. March-Russell, String axiverse, Phys. Rev. D **81**, 123530 (2010).
[172] A. Arvanitaki and S. Dubovsky, Exploring the string axiverse with precision black hole physics, Phys. Rev. D **83**, 044026 (2011).
[173] D. Baumann, H. S. Chia, and R. A. Porto, Probing ultralight bosons with binary black holes, Phys. Rev. D **99**, 044001 (2019).
[174] D. Baumann, H. S. Chia, R. A. Porto, and J. Stout, Gravitational collider physics, Phys. Rev. D **101**, 083019 (2020).
[175] D. Baumann, H. S. Chia, J. Stout, and L. ter Haar, The spectra of gravitational atoms, J. Cosmol. Astropart. Phys. 12 (2019) 006.
[176] D. Baumann, G. Bertone, J. Stout, and G. M. Tomaselli, Ionization of gravitational atoms, Phys. Rev. D **105**, 115036 (2022).
[177] A. Foschi *et al.* (GRAVITY Collaboration), Using the motion of S2 to constrain scalar clouds around Sgr A*, Mon. Not. R. Astron. Soc. **524**, 1075 (2023).
[178] E. Cannizzaro, L. Sberna, S. R. Green, and S. Hollands, Relativistic perturbation theory for black-hole boson clouds, Phys. Rev. Lett. **132**, 051401 (2024).
[179] E. Berti, V. Cardoso, and M. Casals, Eigenvalues and eigenfunctions of spin-weighted spheroidal harmonics in four and higher dimensions, Phys. Rev. D **73**, 024013 (2006); **73**, 109902(E) (2006).
[180] R. A. Konoplya and A. V. Zhidenko, Decay of massive scalar field in a Schwarzschild background, Phys. Lett. B **609**, 377 (2005).
[181] E. Franzin, S. Liberati, and M. Oi, Superradiance in Kerr-like black holes, Phys. Rev. D **103**, 104034 (2021).
[182] P. H. C. Siqueira and M. Richartz, Quasinormal modes, quasibound states, scalar clouds, and superradiant instabilities of a Kerr-like black hole, Phys. Rev. D **106**, 024046 (2022).
[183] S. R. Dolan, Instability of the massive Klein-Gordon field on the Kerr spacetime, Phys. Rev. D **76**, 084001 (2007).
[184] Y. Huang, D.-J. Liu, X.-h. Zhai, and X.-z. Li, Instability for massive scalar fields in Kerr-Newman spacetime, Phys. Rev. D **98**, 025021 (2018).
[185] S. Hod and O. Hod, Analytic treatment of the black-hole bomb, Phys. Rev. D **81**, 061502 (2010).
[186] S. Hod, Kerr-Newman black holes with stationary charged scalar clouds, Phys. Rev. D **90**, 024051 (2014).
[187] Y. Huang and D.-J. Liu, Scalar clouds and the superradiant instability regime of Kerr-Newman black hole, Phys. Rev. D **94**, 064030 (2016).
[188] T. Damour, N. Deruelle, and R. Ruffini, On quantum resonances in stationary geometries, Lett. Nuovo Cimento **15**, 257 (1976).
[189] T. J. M. Zouros and D. M. Eardley, Instabilities of massive scalar perturbations of a rotating black hole, Ann. Phys. (N.Y.) **118**, 139 (1979).

[190] S. L. Detweiler, Klein-Gordon equation and rotating black holes, Phys. Rev. D **22**, 2323 (1980).
[191] E. Berti and K. D. Kokkotas, Quasinormal modes of Kerr-Newman black holes: Coupling of electromagnetic and gravitational perturbations, Phys. Rev. D **71**, 124008 (2005).
[192] R. A. Konoplya and A. Zhidenko, Stability and quasinormal modes of the massive scalar field around Kerr black holes, Phys. Rev. D **73**, 124040 (2006).
[193] R. A. Konoplya and A. Zhidenko, Massive charged scalar field in the Kerr-Newman background I: Quasinormal modes, late-time tails and stability, Phys. Rev. D **88**, 024054 (2013).
[194] E. W. Leaver, An analytic representation for the quasi normal modes of Kerr black holes, Proc. R. Soc. A **402**, 285 (1985).
[195] M. J. Strafuss and G. Khanna, Massive scalar field instability in Kerr spacetime, Phys. Rev. D **71**, 024034 (2005).
[196] J. G. Rosa, The extremal black hole bomb, J. High Energy Phys. 06 (2010) 015.
[197] S. R. Dolan, Superradiant instabilities of rotating black holes in the time domain, Phys. Rev. D **87**, 124026 (2013).
[198] H. Furuhashi and Y. Nambu, Instability of massive scalar fields in Kerr-Newman space-time, Prog. Theor. Phys. **112**, 983 (2004).
[199] H. S. Vieira, V. B. Bezerra, and C. R. Muniz, Instability of the charged massive scalar field on the Kerr–Newman black hole spacetime, Eur. Phys. J. C **82**, 932 (2022).
[200] D. Liu, Y. Yang, A. Övgün, Z.-W. Long, and Z. Xu, Gravitational ringing and superradiant instabilities of the Kerr-like black holes in a dark matter halo, Eur. Phys. J. C **83**, 565 (2023).
[201] H.-P. Nollert, Quasinormal modes of Schwarzschild black holes: The determination of quasinormal frequencies with very large imaginary parts, Phys. Rev. D **47**, 5253 (1993).
[202] J. L. Jaramillo, R. Panosso Macedo, and L. Al Sheikh, Pseudospectrum and black hole quasinormal mode instability, Phys. Rev. X **11**, 031003 (2021).
[203] A. Ohashi and M.-a. Sakagami, Massive quasi-normal mode, Classical Quantum Gravity **21**, 3973 (2004).
[204] R. A. Konoplya, Massive vector field perturbations in the Schwarzschild background: Stability and unusual quasinormal spectrum, Phys. Rev. D **73**, 024009 (2006).
[205] A. Zhidenko, Massive scalar field quasi-normal modes of higher dimensional black holes, Phys. Rev. D **74**, 064017 (2006).
[206] K. D. Kokkotas, R. A. Konoplya, and A. Zhidenko, Bifurcation of the quasinormal spectrum and zero damped modes for rotating dilatonic black holes, Phys. Rev. D **92**, 064022 (2015).
[207] S. Hod, Quasi-bound states of massive scalar fields in the Kerr black-hole spacetime: Beyond the hydrogenic approximation, Phys. Lett. B **749**, 167 (2015).
[208] S. Hod, Slowly decaying resonances of charged massive scalar fields in the Reissner-Nordström black-hole spacetime, Phys. Lett. B **761**, 53 (2016).
[209] R. A. Konoplya and A. Zhidenko, Quasinormal modes of massive fermions in Kerr spacetime: Long-lived modes and the fine structure, Phys. Rev. D **97**, 084034 (2018).
[210] R. A. Konoplya, A. F. Zinhailo, and Z. Stuchlík, Quasinormal modes, scattering, and Hawking radiation in the vicinity of an Einstein-dilaton-Gauss-Bonnet black hole, Phys. Rev. D **99**, 124042 (2019).
[211] M. S. Churilova, R. A. Konoplya, and A. Zhidenko, Arbitrarily long-lived quasinormal modes in a wormhole background, Phys. Lett. B **802**, 135207 (2020).
[212] J. Percival and S. R. Dolan, Quasinormal modes of massive vector fields on the Kerr spacetime, Phys. Rev. D **102**, 104055 (2020).
[213] W. Xiong, P. Liu, C.-Y. Zhang, and C. Niu, Quasinormal modes of the Einstein-Maxwell-aether black hole, Phys. Rev. D **106**, 064057 (2022).
[214] H. Yang, F. Zhang, A. Zimmerman, D. A. Nichols, E. Berti, and Y. Chen, Branching of quasinormal modes for nearly extremal Kerr black holes, Phys. Rev. D **87**, 041502 (2013).
[215] H. Yang, A. Zimmerman, A. Zenginoğlu, F. Zhang, E. Berti, and Y. Chen, Quasinormal modes of nearly extremal Kerr spacetimes: Spectrum bifurcation and power-law ringdown, Phys. Rev. D **88**, 044047 (2013).
[216] H. Onozawa, T. Mishima, T. Okamura, and H. Ishihara, Quasinormal modes of maximally charged black holes, Phys. Rev. D **53**, 7033 (1996).
[217] M. Richartz, Quasinormal modes of extremal black holes, Phys. Rev. D **93**, 064062 (2016).
[218] O. J. C. Dias, M. Godazgar, J. E. Santos, G. Carullo, W. Del Pozzo, and D. Laghi, Eigenvalue repulsions in the quasinormal spectra of the Kerr-Newman black hole, Phys. Rev. D **105**, 084044 (2022).
[219] O. J. C. Dias, M. Godazgar, and J. E. Santos, Eigenvalue repulsions and quasinormal mode spectra of Kerr-Newman: An extended study, J. High Energy Phys. 07 (2022) 076.
[220] S. Sarkar, M. Rahman, and S. Chakraborty, Perturbing the perturbed: Stability of quasinormal modes in presence of a positive cosmological constant, Phys. Rev. D **108**, 104002 (2023).
[221] J. C. S. Neves and C. Molina, Rotating black holes in a Randall-Sundrum brane with a cosmological constant, Phys. Rev. D **86**, 124047 (2012).
[222] D. Baumann, G. Bertone, J. Stout, and G. M. Tomaselli, Sharp signals of boson clouds in black hole binary inspirals, Phys. Rev. Lett. **128**, 221102 (2022).
[223] G. M. Tomaselli, T. F. M. Spieksma, and G. Bertone, Dynamical friction in gravitational atoms, J. Cosmol. Astropart. Phys. 07 (2023) 070.
[224] T. Takahashi, H. Omiya, and T. Tanaka, Axion cloud evaporation during inspiral of black hole binaries: The effects of backreaction and radiation, Prog. Theor. Exp. Phys. **2022**, 043E01 (2022).
[225] T. Takahashi, H. Omiya, and T. Tanaka, Evolution of binary systems accompanying axion clouds in extreme mass ratio inspirals, Phys. Rev. D **107**, 103020 (2023).

[226] J. Zhang and H. Yang, Gravitational floating orbits around hairy black holes, Phys. Rev. D **99**, 064018 (2019).
[227] J. Zhang and H. Yang, Dynamic signatures of black hole binaries with superradiant clouds, Phys. Rev. D **101**, 043020 (2020).
[228] X. Tong, Y. Wang, and H.-Y. Zhu, Termination of superradiance from a binary companion, Phys. Rev. D **106**, 043002 (2022).
[229] K. Fan, X. Tong, Y. Wang, and H.-Y. Zhu, Modulating binary dynamics via the termination of black hole superradiance, Phys. Rev. D **109**, 024059 (2024).
[230] R. Cayuso, O. J. C. Dias, F. Gray, D. Kubizňák, A. Margalit, J. E. Santos, R. Gomes Souza, and L. Thiele, Massive vector fields in Kerr-Newman and Kerr-Sen black hole spacetimes, J. High Energy Phys. 04 (2020) 159.